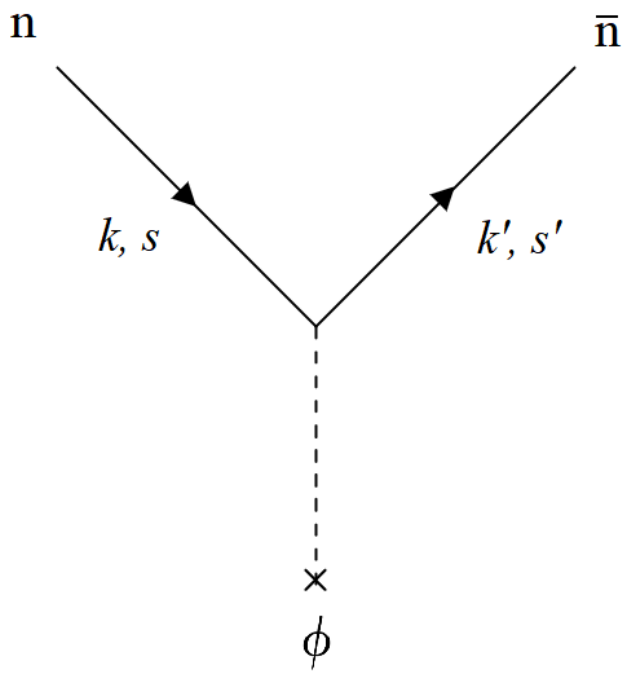

Searching for Scalar Wave Dark Matter with Levitated Magnetomechanics

Sensitivity Studies for a Hypothetical Direct Detection Experiment Using Superconducting Levitating Objects

Master's thesis in Physics

AMANDA CARLSSON SALOMON

DEPARTMENT OF PHYSICS
CHALMERS UNIVERSITY OF TECHNOLOGY
Gothenburg, Sweden 2023
www.chalmers.se

Master's thesis 2023

Searching for Scalar Wave Dark Matter with Levitated Magnetomechanics

Sensitivity Studies for a Hypothetical Direct Detection Experiment Using Superconducting Levitating Objects

AMANDA CARLSSON SALOMON

CHALMERS
UNIVERSITY OF TECHNOLOGY

Department of Physics
Division of Subatomic, High Energy and Plasma Physics
Theoretical Subatomic Physics Group
Chalmers University of Technology
Gothenburg, Sweden 2023

Searching for Scalar Wave Dark Matter with Levitated Magnetomechanics
Sensitivity Studies for a Hypothetical Direct Detection Experiment Using Superconducting Levitating Objects
AMANDA CARLSSON SALOMON

Supervisor: Riccardo Catena, Department of Physics
Examiner: Riccardo Catena, Department of Physics

Master's Thesis 2023
Department of Physics
Division of Subatomic, High Energy and Plasma Physics
Theoretical Subatomic Physics Group
Chalmers University of Technology
SE-412 96 Gothenburg
Telephone +46 31 772 1000

Cover: Feynman diagram for a neutron scattering of a classical scalar dark matter field.

Typeset in LaTeX
Printed by Chalmers Reproservice
Gothenburg, Sweden 2023

Searching for Scalar Wave Dark Matter with Levitated Magnetomechanics
Sensitivity Studies for a Hypothetical Direct Detection Experiment Using Superconducting Levitating Objects
AMANDA CARLSSON SALOMON
Department of Physics
Chalmers University of Technology

Abstract

This thesis investigates the light scalar boson, with mass between $1.24 \cdot 10^{-13}$ and $4.14 \cdot 10^{-12}$ eV, as a wave dark matter candidate. For such low masses, the bosons can be described as a classical wave instead of individual particles, which motivates a field description of the dark matter. The scalar boson is assumed to interact only with neutrons in a charge-neutral test object, giving it a time-dependent EP-violating acceleration that can be detected in a direct detection experiment. The focus of this thesis was to develop a theoretical and statistical framework for the scalar boson by deriving this EP-violating acceleration, and applying the principle of detection to a potential experiment at Chalmers University of Technology using levitated magnetomechanics. The achievable experimental sensitivity could then be estimated for the hypothetical experiment with analytic derivations of exclusion and discovery limits for the scalar-neutron coupling constant. The purpose of the limits was to determine for which values of the coupling constant the dark matter candidate could be detected or not, and they were derived analytically with the help of a likelihood formalism utilising the so called Asimov data set. Comparing the results with a similar analysis done for the same dark matter candidate, the achievable sensitivity for the proposed magnetic levitation experiment could be concluded to be relatively high.

Keywords: Wave dark matter, light dark matter, scalar boson, EP-violation, direct detection, levitated magnetomechanics, experimental sensitivity, Asimov data set, exclusion limit, discovery limit.

Acknowledgements

First of all I would like to thank my supervisor Riccardo Catena for giving me this opportunity to write my Master's thesis with him during this last year. His support, knowledge and guidance have been invaluable to this project. I would also like to thank Witlef Wieczorek and his research group for the valuable insight into their experiment that made this project all the more exciting for the opportunity to test theory on reality. Finally, I would also like to thank Måns Anduri for much support and discussion, giving me a boost and change of perspective when I needed it.

Amanda Carlsson Salomon, Gothenburg, November 2023

Contents

List of Acronyms

Below is the list of acronyms that have been used throughout this thesis listed in alphabetical order:

ALP	Axion Like Particle
CDF	Cumulative Distribution Function
CP	Charge conjugation and Parity
DM	Dark Matter
EP	Equivalence Principle
LHC	Large Hadron Collider
MACHO	Massive Astrophysical Compact Halo Objects
PDF	Probability Density Function
PSD	Power Spectral Density
QM	Quantum Mechanics
QFT	Quantum Field Theory
QTL	Quantum Technology Laboratory
SHM	Standard Halo Model
WEP	Weak Equivalence Principle
WIMP	Weakly Interacting Massive Particle
WMAP	Wilkinson Microwave Anisotropy Probe

List of Figures

1
Introduction

Dark matter is one of the most elusive mysteries in astrophysics and cosmology. While there is a large amount of evidence for its existence, the nature of it is still unknown. In particle physics, dark matter particles are actively searched for, both in colliders and dark matter detection experiments, but no such particles have as of yet been discovered [1]. To detect dark matter would be one of the greatest achievements in modern physics, as it would confirm an hypothesis decades long in the making and supported by a large amount of evidence. A variety of dark matter theories and candidates exists, and while many candidates have already been dismissed as unlikely, many are also still examined and tested. One candidate which has not been tested as much is the scalar boson, a type that stems from the wave dark matter theory in which dark matter is believed to behave classically wave-like. This candidate is explained and examined in the following thesis, based on a theoretical model that is constructed in Chapter 2.

Before going into the scalar dark matter theory, however, this chapter gives an overview of the history of dark matter that has lead up to today's theories. First the evidence for dark matter is explained, followed by some of the most popular dark matter candidates over the years up until today. Then a short description of searches for dark matter and detection experiments is given. Finally, a thorough thesis description is made, explaining the details of how the scalar candidate is tested, as well as making a connection to a hypothetical detection experiment.

1.1 History of dark matter

The history of dark matter is usually centred around two contributors: Fritz Zwicky and his work on galaxy clusters in the 1930s, and the work of Vera Rubin on galactic rotation curves in the 1970s [2]. While their research can be said to be the main foundation for evidence of dark matter, the historical path that lead them to their findings is much longer and the scientific discoveries that followed are still not entirely understood by today's scientists. A brief summary of the history that led Zwicky and Rubin to their discoveries will be given here, and the interested reader is referred to [2] for a more complete account.

While the existence of what is today called dark matter has not been known for more than a century, scientific work since the 1700s have contributed to the discovery of it. During the 1700s and 1800s astronomers and mathematicians made predictions

of the existence of invisible astrophysical objects, using the published work of Isaac Newton on gravity and motion in 1687, many of which were later observationally proven to be correct. Then, with the invention of astronomical photography in the 1800s, astronomers got their first glimpse of the uneven stellar distribution and dark structures in the sky. The discovery of these dark regions prompted many questions and one of the leading hypothesis to what they were was that there was some type of matter that absorbed the light in the line of sight – a "dark" matter.

1.1.1 Evidence for dark matter

While astronomers in the 1800s suspected that there could be non-visible matter in the Universe, it was far from certain and little evidence had as of then been found. But that was about to change in the 1930s, when two astronomers made observations of galaxy clusters that gave a strong indication to the existence of a "missing" mass. Following this, observations of flat galactic rotation curves solidified the belief in the existence of dark matter.

1.1.1.1 Galaxy clusters and galaxy masses

Fritz Zwicky studied the redshift of galaxy clusters, in particular the Coma cluster, which exhibited a large velocity dispersion compared to other clusters. This had already been observed, but none had a good answer for why. In his attempt to explain this, Zwicky applied the virial theorem to the cluster in order to estimate its mass, using the average mass of 10^9 $M_\odot$ (solar masses) per galaxy as suggested by Edwin Hubble. With a size estimation of 10^6 light-years of the spherical cluster system and 800 observed galaxies, he calculated that the system should have a velocity dispersion of 80 km/s. But what he observed was an average velocity dispersion of about 1000 km/s, from which he concluded that there appeared to be a much larger amount of "dark" matter than luminous matter in the cluster. This was one of the first concrete signs of existing non-visible matter in the Universe.

Zwicky continued his study of the Coma cluster and in 1937 he instead tried to estimate the average mass of the galaxies, now assuming that the cluster contained 1000 galaxies within a radius of $2 \cdot 10^6$ light-years and using the observed velocity dispersion of 700 km/s. He obtained an average galaxy mass of $4.5 \cdot 10^{10}$ $M_\odot$, somewhat higher than Hubble's proposal. Assuming an average absolute luminosity of $8.5 \cdot 10^7$ $L_\odot$ (solar luminosities) for cluster galaxies, he arrived at an estimated mass-to-light ratio of approximately 500. With today's more exact values of the Hubble constant than the one Zwicky used to relate redshift and distance, results show that his estimated mass-to-light ratio was too large by a factor of about 8.3. Despite this error, however, a very high mass-to-light ratio is still implied, which indicates the existence of some form of "dark" matter.

At about the same time, Sinclair Smith studied the Virgo cluster and estimated the average mass per galaxy to about 100 times larger than that calculated by Hubble a few years earlier, which presented astronomers with a problem. A very large amount of non-visible matter seemed to be needed in galaxies to explain their high mass,

which many thought was unlikely. Many solutions were suggested, among others that the more massive galaxies found were not permanent members of the clusters, but none of them were entirely satisfactory. Yet, while the "dark" matter theory was not accepted, it was not entirely rejected either and scientist began to speculate on what this missing mass could be.

1.1.1.2 Rotation curves of galaxies

The flatness of galactic rotation curves at large radial distance from the galactic centre has probably been the most convincing piece of evidence for dark matter in astronomical observations [2]. The rotation curve of a galaxy is a way of showing the circular velocity at different radii, and by studying its form one can infer the mass distribution of the galaxy. In ordinary Keplerian systems, such as planetary systems, the rotational velocity of objects decline with distance from the centre, reflecting the decreasing mass distribution of the systems [3]. Galaxies, however, do not have this Keplerian fall-off in velocity. The rotational velocity is constant far from the centre all the way out to the largest radii of the galaxy, giving a flat rotation curve [1]. This is illustrated in fig. 1.1 (from [4]), where the rotation curves for spiral galaxies of various luminosities are seen to level off further from the galactic centre. The flat profile so far from the galactic centre reflects that the mass distribution increases with the radius, indicating that there is a large amount of matter in the outer regions of the galaxy.

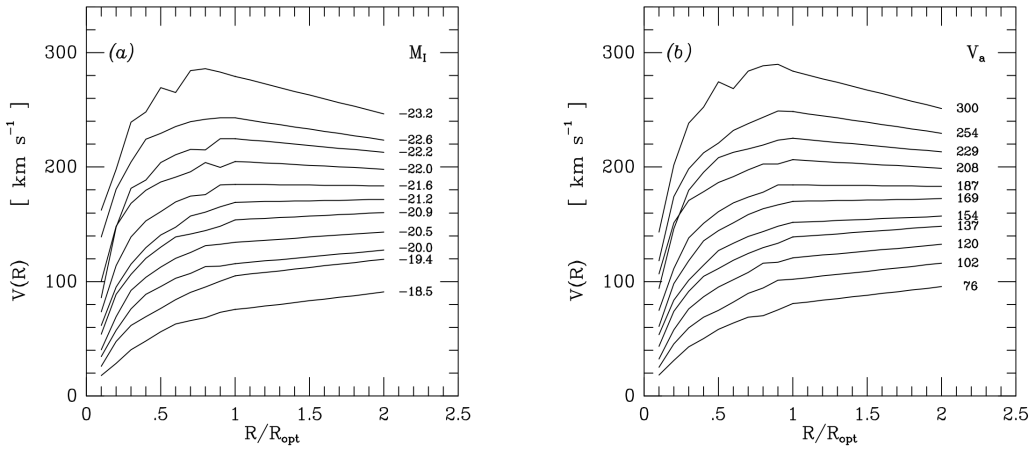

Figure 1.1: Rotation curves of high luminosity spiral galaxies shown to the left, and low luminosity spiral galaxies to the right. Rotational velocity is plotted against the optical radius R_{opt} describing the extension of the luminous matter in the disc. Credit: Persic et al. (1999).

The first clear arguments of flat rotation curves indicating the existence of what is today called dark matter began to appear in the 1970s, based on observations of galaxies done both in the optical and radio range [2]. The optical observations could only provide rotation curves as far out as the visible radii of galaxies, but

even within this range the flat profile was visible. This pointed at the existence of some invisible matter – dark matter – within the visible part of the galaxy at least. The most famous work done on rotation curves with optical observations is that of Vera Rubin, Kent Ford and Norbert Thonnard in 1978, in which they constructed rotation curves for ten highly luminous spiral galaxies, all of them with clear flat profiles [2, 5]. With radio observations, however, the flat rotation curve could be shown to extend beyond the visible radius of the galaxy, giving strong indications for some invisible mass extending further out than just the visible stars and gas – a dark matter halo. The collective evidence from galaxy cluster observations and galactic rotation curves now clearly pointed at the existence of dark matter.

1.1.2 Dark matter candidates

Having been largely accepted in the physics community, dark matter became an established term for the particles making up the majority of the mass in the Universe that had previously been unaccounted for, as opposed to "dark" meaning objects too faint to be detected with available telescopes. Yet the nature of dark matter was still unknown, and by the late 1980s the most popular theory became that dark matter was some yet-unknown subatomic particle or particles, a hypothesis that still stands strong today. A number of dark matter candidates have been suggested, but not all are compatible with observations of the Universe.

1.1.2.1 Neutrinos

The neutrinos of the standard model were some of the first dark matter candidates to be considered, as they exhibit the most important characteristics for a viable dark matter candidate: they are long lived and do not interact electromagnetically or strongly [2]. There is, however, a problem with these candidates that relates to the structure formation of the Universe.

The development of numerical simulations in the 1980s made it possible to predict the evolution of a large number of dark matter particles influenced by gravity in an early expanding Universe [2]. This allowed scientists to discriminate between some of the dark matter candidates based on the evolution of large scale structures. In simulations, the most important characteristic for a given dark matter candidate is whether it was relativistic, hot, or non-relativistic, cold, when structure formation took place in the Universe [2]. The standard model neutrinos were very abundant in the early evolution of the Universe, but only those with very high temperature, and thus energy, in order to maintain an equilibrium between the creation and annihilation of neutrinos [6]. These were therefore predicted to have been highly relativistic in the early Universe, and are thus an example of hot dark matter.

Numerical simulations show that if dark matter was hot, it would tend to collapse first and form very large structures, and then later fragment into smaller structures, such as galaxy-sized halos [2]. If it was cold, however, dark matter would form smaller structures first and later larger structures through mergers. Cosmological observations, such as [7], show that in order to explain the apparent structure of the

Universe, small scale structures will have had to appear first, evolving into larger scale structures. That makes the standard model neutrinos, or any hot dark matter, unlikely as candidates. While hot dark matter could still exist, it cannot be what makes up the dark matter in galactic halos important for structure formation. Some other type of cold dark matter is therefore needed to explain this.

1.1.2.2 WIMPs

When dark matter began to be discovered, a strong theory was that it consisted of massive astrophysical compact halo objects – MACHOs – that was just normal baryonic matter but with very low luminosity [2]. With the discovery of the cosmic microwave background in 1965 and an increased interest in the Big Bang nucleosynthesis, however, the cosmological baryon density began to be a subject of interest [1, 2]. Measuring the baryon density would prove to be the final evidence that also showed the non-baryonic nature of dark matter.

The first restraints on the baryon density were done in the 1970s and has since then been refined considerably [2]. Most recently, the Planck Collaboration's analysis of data collected with WMAP [8] gave a restraint on the baryon density that, when compared to the total matter density, inferred that less than 20% of matter is baryonic in the Universe. With this fact, the conclusion became that dark matter could not be baryonic in nature, strengthening the hypothesis of dark matter being some unknown subatomic particle [2].

Based on previously mentioned restriction of the majority of dark matter needing to be cold, together with it being long lived and at most only weakly interacting, the leading candidates are weakly interacting massive particles – WIMPs [2]. With masses in the MeV-TeV range, there are several WIMP candidates that over the years have been thoroughly studied theoretically and many experiments have been made in search of evidence for WIMPs.

In classifying dark matter candidates, there is another important distinction made in whether the dark matter is thought to have been created thermally or non-thermally in the early Universe [9]. WIMPs are an example of thermally created dark matter. They would have been created in very large amounts and in the early epochs of the Universe they would have been in thermal equilibrium, annihilation and creation processes happening at equal rates. As the Universe expanded and temperatures dropped below the WIMP mass, production would stop and as expansion continued annihilations would also cease due to the increased spatial separation of the dark matter particles [10], causing a "freeze-out" of the dark matter density. For this freeze-out to have given today's measured relic abundance of dark matter, the particle mass would have to be in the MeV-TeV range as for WIMPs. But that does not exclude the possibility of lighter particles as dark matter; they just have to have been created differently.

1.1.2.3 Axions and ALPs

Non-thermal creations of cold dark matter would require either production at low temperatures, without thermal equilibrium, or an extremely weak interaction with the surrounding plasma so as to be effectively decoupled from it [1]. As an example of a non-thermally created dark matter candidate, the axion, with mass less than 10^{-3} eV, is probably the most well-known. It was first introduced to solve the strong CP-problem in quantum chromodynamics, but being stable over large timescales and expected to be extremely weakly interacting, it could also constitute the dark matter [2, 3]. Accurate calculations of expected axion relic density depends on the production mechanism assumed, for which there are a few suggestions, but it is still possible to get a density range for which the axion satisfy all necessary constraints to be a dark matter candidate.

The axion has in turn lead to the theory of axion-like particles (ALPs) as dark matter, also non-thermally created and with very small masses. The difference between the original axion and ALPs essentially lies in whether their small mass comes from non-perturbative effects or explicit symmetry breaking, but they are both equally fitting cold dark matter candidates [11]. A question one could ask, however, is whether particles this light could be non-relativistic and hence cold [1]. Neutrinos, for example, were thermally created and are expected to have decoupled from the surrounding plasma at high temperatures due to its tiny mass, which would make them relativistic. But since axions and ALPs were non-thermally created, non-relativistic velocities would not be a problem to produce, making them still viable cold dark matter candidates.

1.1.2.4 Wave dark matter

Axions and ALPs are both examples of very light dark matter candidates and can be grouped into a category of dark matter models called wave dark matter [12]. This is a group that has gotten more attention recently, and a number of candidates have risen from it, one of which is the focus of this thesis. What all wave dark matter candidates have in common is that they are bosons with masses below the eV scale. The difference between these type of candidates and the previously mentioned ones is that since they have such small masses, they can be viewed as waves rather than as individual particles, allowing for a field description of dark matter.

The theory behind wave dark matter models will be explained in more detail in Section 2.1, as it will be central to building up the theory of the dark matter candidate of this thesis. In general, though, wave dark matter models have the advantage of the wave description on galactic scales, making for easier theoretical analyses of small-scale observations and even allowing for non-cold dark matter behaviour on small scales. On large scales, however, the dark matter still behaves like cold dark matter, fitting current theories on structure formation. Candidates of this type are therefore extremely versatile since the wave nature of them offers a rich new phenomenology.

1.1.3 Searches for dark matter

Even though the exact nature of dark matter remains a mystery, searching for dark matter candidates has become an increasingly large field in experimental physics. Detecting it would be the best way to prove the dark matter hypothesis, and could also answer the question: what is dark matter? Possible detection experiments have been discussed since the late 1970s and many are tested today [2]. When searching for dark matter, there are three processes to consider that are either detectable or give detectable products [2, 13]. Detection can be done directly or indirectly depending on which process that is being considered, but all three processes are dependent on how dark matter couples to ordinary matter.

1.1.3.1 Collider production and annihilation or decay products

One process to consider is the production of dark matter particles when colliding standard model particles in particle accelerators [13]. Experiments at LHC have for example been colliding protons in the hope of detecting new particles since 2008, resulting in the discovery of the Higgs boson. To infer the presence of dark matter in such collisions, one would need to observe events with missing transferred momentum and energy. While this has yet to occur, the search for such events continue.

Apart from standard model particles producing dark matter particles in colliders, the reverse could also be detectable via dark matter self-annihilation or decay [13]. The annihilation or decay of dark matter particles into standard model particles could produce a measurable particle flux, and measuring this flux would constitute as an indirect detection of dark matter. Mostly, the additional decay of these annihilation or decay products into gamma rays, neutrinos, electron or proton pairs would give the observable flux that is searched for in indirect detection experiments.

These indirect signals of particle or gamma ray fluxes are searched for in astrophysical objects, such as stars and galaxies, where dark matter has gravitationally accumulated and the increased dark matter density can produce a measurable flux [13]. Searches for gamma ray fluxes were proposed as early as 1978 [2], and recently the search for neutrino fluxes from the Sun has been given a lot of attention.

1.1.3.2 Direct detection of scattering processes

The third process to consider is dark matter scattering of nuclei [13]. Searches involving this process use direct detection methods that look for direct effects of this interaction. A lot of attention has been put recently on designing experiments that use this method, mainly looking for elastic scattering of WIMPs.

When using direct detection in scattering processes to look for dark matter particles, any detectable signal produced in the process will depend on the type of interaction between the dark matter and the target of the scattering [14]. When looking at experiments involving WIMPs scattering elastically of nuclei, one seeks to detect the nuclear recoils caused by the WIMP interacting with neutrons or protons in a

detector. When searching for lighter dark matter candidates in the sub-GeV range, however, the effect of the particle interaction with the individual nucleons in the detector would be to small to detect. Instead most models suggest looking for light dark matter scattering of electrons, which could give a detectable signal [13]. So far, though, no such signal of either kind has been detected.

In the case of wave dark matter, however, one could actually use nuclear recoil experiments to search for dark matter signals. As individual particles, the dark matter would not be able to produce a detectable nuclear recoil signal, but due to its wave nature a signal could be detected by the dark matter field interacting with the whole detector. Such experiments have not been explored much, but there are suggestions, for example in [15], on how one could proceed in this direction.

1.2 Thesis motivation

The interest of searching for wave-like dark matter in direct detection experiments involving nuclear scattering is what motivates this thesis. With a light scalar boson, with mass in the sub-eV range, as a dark matter candidate, this thesis seeks to analyse the experimental sensitivity of a hypothetical direct detection experiment at Chalmers University of Technology. The experiment under consideration would be performed in the Quantum Technology Laboratory (QTL) at MC2, in which current research includes levitating superconductive micro-particles [16]. The set-up would consist of a test object in the form of a superconductive lead micro-sphere being levitated in a superconducting magnetic trap [17]. The suggested scalar boson candidate is assumed to interact only with the neutrons in the test object, inducing a time-dependent equivalence-principle violating acceleration of the the test object. This acceleration can then in theory be detected by measuring the motion of the levitated micro-sphere.

Details of the suggested experimental set-up can be found in [17], but the main parts include a magnetic trap, in which the superconducting test object levitates. The trap is constructed of two superconducting coils in which a current flows, generating a magnetic field with the test object levitating near the minimum of the field. The motion of the object is detected via two pickup loops, where the current induced in the loops changes as the magnetic flux threading the loops changes due to the object's motion. The flux is then transduced into a measurable voltage via a commercial dc-SQUID magnetometer connected to the pickup loops.

Two sizes of the test object are considered; one that of a lead sphere with radius 1 µm and mass $5 \cdot 10^{-14}$ kg, and the other a sphere with radius 100 µm and mass $5 \cdot 10^{-8}$ kg. The test object is assumed to be levitated at a temperature of $T_{\text{temp}} = 10$ mK, with a trap frequency of $\omega_{\text{t}}/(2\pi) = 100$ Hz, and two values of the mechanical quality factor Q_{m} are assumed: 10^7 and 10^{11}. The test object is also assumed to be subject to a thermally-limited acceleration noise given by:

$$S_{aa}^{\text{therm}} = \frac{4k_{\text{B}}\omega_{\text{t}}T_{\text{temp}}}{Q_{\text{m}}m_{\text{t.o}}}, \tag{1.1}$$

with k_{B} being the Boltzmann constant and $m_{\text{t.o}}$ the mass of the test object. With two values of the quality factor and two sizes of the test object, four different thermal noise contributions can be considered. This noise is used as a background term in the analytical testing of the dark matter model constructed in Chapter 2.

In modelling the scalar dark matter, a likelihood function-based framework is used to relate the theoretical descriptions in the model to a detectable signal in a hypothetical experiment. The theoretical dark matter induced acceleration of the test object is derived in Chapter 2, based on the work in [15], after which a likelihood function is derived in Chapter 3 with this acceleration as input, based on the work in [18]. Using the likelihood, the experimental sensitivity of the proposed experiment is calculated with pure analytical methods. This is done in Chapter 4, in which statistical tools are constructed that make analytic predictions of exclusion and discovery limits of the scalar-neutron coupling constant describing the interaction strength between the dark matter and neutrons. The limits of the coupling constant needed to either exclude the possibility of a signal or confirm discovery of a signal are calculated in Chapter 5, with experiment dependent parameter values set according to the proposed experiment at QTL. Natural units are used throughout the thesis unless otherwise stated.

2
Modelling the dark matter

The following chapter gives an overview of the light bosonic dark matter model, explaining the bosonic and wave-like nature of the dark matter candidate under consideration, as well as showing how the dark matter couples to neutrons. The chapter ends with a concrete description of the EP-violating acceleration of interest for the detection experiment discussed previously, resulting in an expression for the acceleration used in the likelihood framework of the next chapter.

2.1 The light bosonic dark matter model

When modelling dark matter, dynamical measurements are a central part in making a good model that fits with observational results. Measuring the mass density of dark matter is of special interest. A reliable value of the local density in the solar system has long been a goal in astrophysics, since most models of dark matter used for experimental searches has a dependence on the local density value [19]. Several galactic mass models for the Milky Way has been proposed over the years, in which suggested density distributions for both baryonic and dark matter differ. Estimating a local value for the dark matter mass density is therefore difficult, as it will depend on the chosen model. Many different values have been given in literature, ranging from 0.3 GeV/cm^3 [20] to 0.49 GeV/cm^3 [21]. In this thesis the value 0.4 GeV/cm^3 is used, as used in [18].

Given that the local dark matter density ρ_{DM} is known, the average separation between the dark matter particles can be estimated and compared to the de Broglie wavelength of the particles [22]:

$$\lambda_{\mathrm{dB}} = \frac{2\pi}{m_{\mathrm{DM}} v},$$

with m_{DM} being the dark matter particle mass and v the velocity of the dark matter in the galactic halo. For the the local galaxy, the velocity is $v \sim 10^{-3}$, assuming the dark matter has virialised to the galaxy [15]. The de Broglie wavelength can be shown to exceed the particle separation if $m_{\mathrm{DM}} \lesssim 30$ eV [22]. This means that, for $m_{\mathrm{DM}} \ll 30$ eV, the average number of particles in a de Broglie volume, given by

$$N_{\mathrm{dB}} = \lambda_{\mathrm{dB}}^3 \frac{\rho_{\mathrm{DM}}}{m_{\mathrm{DM}}}, \tag{2.1}$$

will be large enough that the particles are best described as classical waves. The classical wave-like behaviour of such light particles motivates a field description of

light dark matter with $m_{\mathrm{DM}} \ll 30$ eV, also called wave dark matter, similar to how the photon can be described by classical electromagnetism. The high occupancy number N_{dB} also implies that wave dark matter must be bosonic in nature, due to the Pauli exclusion principle [22]. Furthermore, the mass needs to be constrained by being approximately $\gtrsim 10^{-22}$ eV, as smaller masses implies that the de Broglie wavelength would be larger than the average size of the smallest observed dark matter dominated galaxies [12]. Lighter particles could exist, but would have to constitute a small fraction of the total dark matter to fit with observations [22]. The lower bound on mass varies in literature and depends on the specifics of the model under consideration, but 10^{-22} eV will be a sufficient lower bound in this thesis, as used in [15].

Describing this bosonic light dark matter as a classical (non-relativistic) field means that an angular oscillation frequency of the field can be introduced, which is commonly identified with energy in quantum mechanics [18]. The full expression for the angular frequency is

$$\omega_{\mathrm{DM}} = m_{\mathrm{DM}} \left(1 + \frac{v^2}{2}\right). \tag{2.2}$$

With a small, non-relativistic velocity $v \sim 10^{-3}$ and masses in the range 10^{-22} eV $\lesssim m_{\mathrm{DM}} \lesssim 1$ eV, the second term in eq. (2.2) can effectively be neglected in favour of the approximation,

$$\omega_{\mathrm{DM}} \approx m_{\mathrm{DM}}, \tag{2.3}$$

as long as one is not specifically interested in studying the velocity distribution of the dark matter [14]. The field description is applicable to all types of light bosonic fields, but to produce concrete results, not all types of bosonic fields are studied here. Even with restricting it to the light part of the spectrum, there are only a few possible types of fields that this model allows the dark matter to be [14]. One of these is the spin-0 scalar boson, which is the focus of this thesis.

2.2 The scalar boson

The coupling and interaction of the scalar boson with the standard model particles give four experimentally detectable effects: spin effects, electromagnetic effects, variations of fundamental constants, and accelerations [14]. The focus here is on the latter; or more specifically, detecting time-dependent equivalence-principle (EP) violating accelerations caused by bosonic dark matter interacting with standard model particles. This acceleration can be detected with the use of a charge-neutral classical test object of ordinary matter that experiences a very small displacement from the dark matter interaction, which is manifested as an EP-violating force on the test object. The force is EP-violating as the coupling with the whole test object is not exactly proportional to the object's mass, which will become apparent in Section 2.2.2.

2.2.1 The interaction potential

The scalar boson can couple to the standard model via derivative and non-derivative interactions [15]. The leading order non-derivative interactions with protons and neutrons, which are Yukawa interactions, will produce the EP-violating force of interest [14]. Assuming that the proton and neutron couplings are different, one could for simplicity and concreteness study the case where one of these couplings is zero and only one interaction contributes to the force. In this thesis, the proton coupling is assumed to be zero, leaving only the scalar-neutron interaction for study. While a coupling to protons would also produce the desired effect, the investigation of scalar-neutron interaction has a wider motive. Although not studied in this thesis, other wave dark matter candidates, such as the vector boson, could also produce a detectable EP-violating force, but then only with neutron coupling [15]. As such, it could be of interest in the future to make a comparison of the EP-violating effect from different dark matter candidates. In addition to this, the scalar-neutron coupling has not been studied much, meaning that results in this thesis could be a new addition to the research field. There are, however, studies made of scalar-quark couplings in general, such as [23] and [24], which can be compared with results here.

For the scalar boson model with only a Yukawa interaction with neutrons, the theory can be described by the Lagrangian:

$$\mathcal{L} = \frac{1}{2}\partial_\mu\phi\partial^\mu\phi - \frac{1}{2}m_\phi^2\phi^2 + y_{\phi n}\phi\bar{n}n. \tag{2.4}$$

Since the dark matter is assumed to be classically wave-like, the scalar field ϕ is a real field and so the first term can be identified as the kinetic term for the scalar field, and the second as the mass term of the boson with mass m_ϕ. The third is the Yukawa interaction with neutrons, represented as n and $\bar{n}$ for the anti-neutron, with coupling constant $y_{\phi n}$.

The scalar-neutron interaction is represented in the S-matrix describing neutrons scattering of an external, classical scalar field. For the case of a single neutron scattering of the space-time-dependent field $\phi(x)$, the S-matrix derived through quantum field theory (QFT) takes the form:

$$S_{fi}^{\mathrm{QFT}} = iy_{\phi n}\int d^4x\phi(x)\langle \overbrace{f|\bar{n}}\overbrace{n|i}\rangle, \tag{2.5}$$

where the interaction Hamiltonian has been taken from the Lagrangian in eq. (2.4), and f and i stand for final and initial state for the neutron, respectively. Note that eq. (2.5) uses Wick contractions, which can be deduced from the first order Feynman diagram of the scattering process in figure 2.1.

Expanding the S-matrix using Feynman rules for fermions (see for example [25]) and notations in figure 2.1 results in:

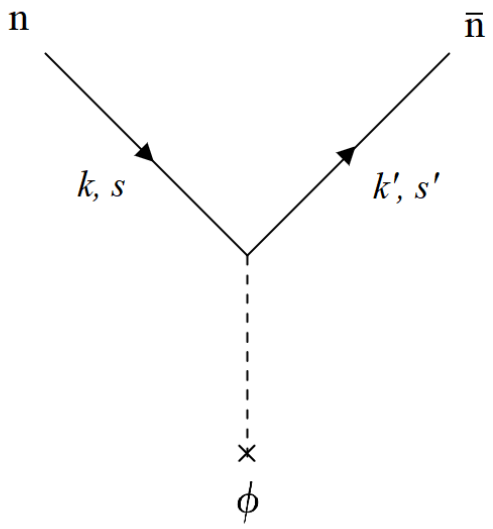

Figure 2.1: Feynman diagram of neutron-scalar scattering process. An incoming neutron n with momentum k and spin s scatters of the classical scalar field ϕ, and the outgoing neutron (here represented as an anti-neutron $\bar{n}$) leaves with momentum k' and spin s'.

$$\begin{aligned} S_{fi}^{\mathrm{QFT}} &= iy_{\phi n} \int d^4x \phi(x) \bar{u}^{s'}(k') e^{ik'\cdot x} \langle 0|u^s(k) e^{-ik\cdot x}|0\rangle \\ &= iy_{\phi n} \int d^4x \phi(x) \bar{u}^{s'}(k') u^s(k) e^{i(k'-k)\cdot x} \\ &= iy_{\phi n} \bar{u}^{s'}(k') u^s(k) \tilde{\phi}(k'-k), \end{aligned} \tag{2.6}$$

where in the last line the transition from position to momentum space has been made, with $\tilde{\phi}(k'-k)$ being the 4-dimensional Fourier transform of the scalar field. The bra and ket vectors $\langle 0|$ and $|0\rangle$ denote the ground states for the anti-neutron and neutron, respectively. To the first order in momenta $\vec{k}$ and $\vec{k}'$, the non-relativistic spin-sum rules for the spinors $\bar{u}^{s'}(k')$ and $u^s(k)$ are $\bar{u}^{s'}(k')u^s(k) \simeq 2m_{\mathrm{n}}\delta^{s's}$, where m_{n} is the mass of the neutron [26]. Eq. (2.6) then reduces to:

$$S_{fi}^{\mathrm{QFT}} \simeq iy_{\phi n} 2m_{\mathrm{n}} \delta^{s's} \tilde{\phi}(k'-k). \tag{2.7}$$

To extract an expression for the Yukawa potential of the scalar-neutron interaction, the S-matrix derived through QFT needs to be compared to the corresponding S-matrix derived from time-dependent perturbation theory in non-relativistic quantum mechanics (QM) (see for example [27]). With the Born approximation, the non-relativistic quantum mechanical expression for the S-matrix with a time-dependent potential then becomes:

$$S_{fi}^{\mathrm{QM}} \simeq -i\tilde{V}(k'-k). \tag{2.8}$$

An expression for the 4-dimensional Fourier transform of the potential can then be extracted through comparison of eqs. (2.7) and (2.8). When comparing, however, $2m_{\mathrm{n}}$ needs to be divided from eq. (2.7), since this is a product of relativistic normalisation of the ground state in QFT. As the neutrons in a neutral test object are unpolarised, the spin is the same before and after the interaction, meaning that $\delta^{s's} = 1$. The 4-dimensional Fourier transform of the potential can then be identified as:

$$\tilde{V}(k' - k) = -y_{\phi n}\tilde{\phi}(k' - k). \tag{2.9}$$

Inverse transforming yields a Yukawa potential of the form

$$V(x) = -y_{\phi n}\phi(x), \tag{2.10}$$

for one neutron scattering of the scalar field $\phi(x)$.

2.2.2 The time-dependent EP-violating acceleration

The force $\vec{F}_\phi$ experienced by a (non-relativistic) neutron in this Yukawa potential can be deduced by writing out the classical Lagrangian for this neutron:

$$\mathcal{L} = \frac{1}{2}m_{\mathrm{n}}|\dot{\vec{x}}|^2 - V(x). \tag{2.11}$$

By applying the Euler-Lagrange equation on this Lagrangian, the sought after force F_ϕ can be identified with the term $m_{\mathrm{n}}|\ddot{\vec{x}}|$ in the resulting equation of motion, leading to the expression

$$\vec{F}_\phi = -\nabla V(x) = y_{\phi n}\nabla\phi(x). \tag{2.12}$$

The force can be seen to depend directly on $\phi(x)$, for which an explicit expression needs to be found. For a real scalar field, the equation of motion for the free field is the Klein-Gordon equation [28]:

$$(\Box + m_\phi^2)\phi(x) = 0. \tag{2.13}$$

The solution to this equation is a time-dependent plane-wave,

$$\phi(x) = Ae^{ik\cdot x} + Be^{-ik\cdot x}, \tag{2.14}$$

for some constants A and B. The wave oscillates with frequency ω_ϕ, which follows eq. (2.2) (but as was argued previously eq. (2.3) is a good approximation as long as one is not interested in quantities of order the size of the frequency spread $\sim m_\phi v^2$). Requiring that the field be real means that eq. (2.14) can be simplified to:

$$\phi(x) = 2A\cos\Big(\omega_\phi t - \vec{k}\cdot\vec{x}\Big). \tag{2.15}$$

The normalisation constant A can be obtained by using the relation between average energy and amplitude for wave dark matter [29]:

$$\rho_{\mathrm{DM}} = \omega_\phi^2|A^2|, \tag{2.16}$$

so that the constant can be seen to be:

$$A = \frac{1}{m_\phi}\sqrt{\frac{\rho_{\mathrm{DM}}}{2}}, \tag{2.17}$$

for $\omega_\phi \approx m_\phi$. This leads to the full expression for the field $\phi(x)$:

$$\phi(x) = \frac{1}{m_\phi}\sqrt{2\rho_{\mathrm{DM}}}\cos\Big(\omega_\phi t - \vec{k}\cdot\vec{x}\Big). \tag{2.18}$$

With eq. (2.12) and the relation $v = |\vec{k}|/\omega_\phi$ between velocity and momentum, the force on a neutron from the dark matter then becomes:

$$|\vec{F}_\phi| = F_\phi = \sqrt{2\rho_{\mathrm{DM}}}\cdot y_{\phi n} v \sin\Big(\omega_\phi t - \vec{k}\cdot\vec{x}\Big). \tag{2.19}$$

The direction of the force will not matter from an experimental point of view, and so only the scalar quantity will be considered. The spatial coordinate of the dark matter field will also be of little consequence as its wave length would be larger than the size of the experiment, and so one can without loss of generality drop the $\vec{x}$ dependence. Then the total time-dependent EP-violating force on a test object containing N_{n} number of neutrons becomes:

$$F_\phi(t) = N_{\mathrm{n}}\sqrt{2\rho_{\mathrm{DM}}}\cdot y_{\phi n} v \sin(\omega_\phi t). \tag{2.20}$$

In an eventual experiment, however, what would be indirectly measured is the acceleration of the test object from this force. The object's mass, $m_{\mathrm{t.o}}$, can be approximated by the number of neutrons plus the number of protons times the neutron mass:

$$m_{\mathrm{t.o}} \approx (N_{\mathrm{n}} + N_{\mathrm{p}})m_{\mathrm{n}}. \tag{2.21}$$

By introducing a material-dependent parameter

$$x_{\mathrm{t.o}} = 1 + \frac{N_{\mathrm{p}}}{N_{\mathrm{n}}}, \tag{2.22}$$

describing the ratio of protons and neutrons in the test object, the mass can be expressed solely in terms of neutron-dependent constants and the parameter $x_{\mathrm{t.o}}$ depending on the specific composition of the test object:

$$m_{\mathrm{t.o}} \approx x_{\mathrm{t.o}} N_{\mathrm{n}} m_{\mathrm{n}}. \tag{2.23}$$

The resulting expression for the acceleration is then:

$$a_\phi(t) = \frac{F_\phi(t)}{m_{\mathrm{t.o}}} \approx \frac{1}{x_{\mathrm{t.o}} m_{\mathrm{n}}}\sqrt{2\rho_{\mathrm{DM}}}\cdot y_{\phi n} v \sin(\omega_\phi t). \tag{2.24}$$

This EP-violating acceleration is used in the next chapter to derive a likelihood function that can be analysed statistically. The analysis, which is done in Chapter 4, determines the experimental sensitivity needed to either detect or reject the possibility of detection of the scalar boson.

3
Likelihood formalism

This chapter gives a description of the likelihood formalism that was used together with the previously derived theoretical framework to analytically estimate the experimental sensitivity of the proposed detection experiment. To search for dark matter in direct detection experiments, one needs to be able to relate the theory with an observable signal. Using the Fourier components of a time-series data as input, one can construct a likelihood function to analyse the data. This is done in [18] and a similar approach was made here, using the same analysis method to interpret statistically inferred results (in Chapter 4) from the derived likelihood function of this chapter.

In this thesis, a hypothetical time-series data was used, consisting of data-points containing information on the displacement of a levitated test object. In other words, the hypothetical data Fourier transformed was the EP-violating acceleration of the test object in the proposed experiment at QTL. Specifically, the actual inputs used in the likelihood function was the power spectral density of the acceleration, which in its definition contains the Fourier transform of the acceleration. This is a useful description of the data, as the spectral shape of the Fourier components contains information on the velocity distribution of the local dark matter in the galactic halo [18].

3.1 Statistics of the scalar field

In order to derive a likelihood function containing statistical information of the local dark matter, the statistics of the scalar field must first be reviewed. A general expression for the scalar field describing the bosonic dark matter was given in eq. (2.18). The local field is, however, comprised of an underlying distribution of fields describing individual bosons. Assuming that there are N_{DM} number of particles making up the local field, each field contribution describing an individual boson will have the form:

$$\phi_i(t) = \frac{1}{m_\phi}\sqrt{\frac{2\rho_{\mathrm{DM}}}{N_{\mathrm{DM}}}}\cos(\omega_i t + \varphi_i), \tag{3.1}$$

where $i \in 1, 2, ..., N_{\mathrm{DM}}$ indexes the field, or mode, identified with a specific dark matter particle. The density has been normalised for an individual particle, and the $\vec{x}$ dependence has been dropped as discussed in Section 2.2.2. For every mode, a random phase $\varphi_i \in [0, 2\pi)$ has also been introduced that describes initial conditions.

The velocity v_i differs for each particle, giving a different angular frequency ω_i for each field which follows equation (2.2). But as stated in Section 2.1, in most cases the approximation $\omega_i \approx m_\phi$ will be sufficient.

The total dark matter induced acceleration experienced by a test object, given in eq. (2.24), can then be expressed as the sum of contributions from each field mode:

$$a_\phi(t) = \sum_i \frac{1}{x_{\mathrm{t.o}} m_{\mathrm{n}}} \sqrt{\frac{2\rho_{\mathrm{DM}}}{N_{\mathrm{DM}}}} y_{\phi n} v_i \sin(\omega_i t + \varphi_i). \tag{3.2}$$

To make it easier to sum over all i, it is advantageous to distribute the total number of particles N_{DM} into subsets Ω_j containing N^j_{DM} particles, as done in [18]. The particles in each subset Ω_j have velocities between v_j and $v_j + \Delta v$, with Δv small enough such that v_j and $v_j + \Delta v$ are effectively indistinguishable. As such, the angular frequency ω_j will be the same for all field modes $\phi_i(t)$ in subset Ω_j, with ω_j as in eq. (2.2). The only thing that differs between the fields in the subset Ω_j will therefore be the random phase φ_i. The acceleration in this subset can then be expressed as:

$$\begin{aligned} a^j_\phi(t) &= \sum_{i \in \Omega_j} \frac{1}{x_{\mathrm{t.o}} m_{\mathrm{n}}} \sqrt{\frac{2\rho_{\mathrm{DM}}}{N_{\mathrm{DM}}}} y_{\phi n} v_j \sin(\omega_j t + \varphi_i) = \\ &= \frac{1}{x_{\mathrm{t.o}} m_{\mathrm{n}}} \sqrt{\frac{2\rho_{\mathrm{DM}}}{N_{\mathrm{DM}}}} y_{\phi n} v_j \,\mathrm{Im}\left\{ e^{i\omega_j t} \left(\sum_{i \in \Omega_j} e^{i\varphi_i} \right) \right\}. \end{aligned} \tag{3.3}$$

The sum over phases is equivalent to a two dimensional random walk, described by a Rayleigh-distributed random number α_j, giving the expression [18, 30]:

$$\sum_{i \in \Omega_j} e^{i\varphi_i} = \alpha_j e^{i\varphi_j}, \tag{3.4}$$

with α_j distributed as:

$$P[\alpha_j] = \frac{2\alpha_j}{N^j_{\mathrm{DM}}} e^{-\alpha_j^2 / N^j_{\mathrm{DM}}}. \tag{3.5}$$

By rescaling $\alpha_j \to \alpha_j \sqrt{N^j_{\mathrm{DM}}/2}$ under probability conservation, the N^j_{DM} dependence can be removed from the distribution, so that the acceleration contribution from field modes in subset Ω_j can be written as:

$$a^j_\phi(t) = \frac{1}{x_{\mathrm{t.o}} m_{\mathrm{n}}} \sqrt{\frac{\rho_{\mathrm{DM}} N^j_{\mathrm{DM}}}{N_{\mathrm{DM}}}} \alpha_j y_{\phi n} v_j \sin(\omega_j t + \varphi_j), \tag{3.6}$$

with α_j distributed as:

$$P[\alpha_j] = \alpha_j e^{-\alpha_j^2/2}. \tag{3.7}$$

To finally sum over all j and get the acceleration from the total local field, it is important to note that the velocities v_j are drawn from the local dark matter velocity distribution. In the standard halo model (SHM), this takes the form [18]:

$$f_{\mathrm{SHM}}(v) = \frac{v}{\sqrt{\pi} v_0 v_{\mathrm{obs}}} e^{-(v+v_{\mathrm{obs}})^2/v_0^2} \cdot (e^{4vv_{\mathrm{obs}}/v_0^2} - 1) \tag{3.8}$$

with $v_0 \approx 220$ km/s being the speed of the local rotation curve, and $v_{\mathrm{obs}} \approx 232$ km/s the speed of the Sun relative to the halo rest frame. Using $f_{\mathrm{SHM}}(v)$, N^j_{DM} can be rewritten as $N^j_{\mathrm{DM}} = N_{\mathrm{DM}} f_{\mathrm{SHM}}(v_j)\Delta v$, which comes from the definition of j. This finally leads to:

$$a_\phi(t) = \frac{1}{x_{\mathrm{t.o}} m_{\mathrm{n}}} \sqrt{\rho_{\mathrm{DM}}} \cdot y_{\phi n} \sum_j v_j \alpha_j \sqrt{f_{\mathrm{SHM}}(v_j)\Delta v} \sin(\omega_j t + \varphi_j) \tag{3.9}$$

for the EP-violating acceleration from the total local dark matter field, with α_j distributed according to (3.7). This expression for the acceleration is equivalent to that of eq. (2.24), but highlights statistical variations of the scalar field needed to analytically estimate the expected sensitivity of an experiment in Chapter 4.

3.2 The likelihood function

As stated in the beginning of this chapter, the form of the hypothetical data needed to analytically construct a likelihood function is a power spectral density (PSD) of the acceleration. This PSD relates the theoretical dark matter induced acceleration of a test object to a observable signal of the scalar boson. The first step of deriving the PSD is defining the following constant:

$$C = \frac{\rho_{\mathrm{DM}}}{x^2_{\mathrm{t.o}} m^2_{\mathrm{n}}} y^2_{\phi n}, \tag{3.10}$$

for ease of notation, so that the acceleration in (3.9) can be written as:

$$a_\phi(t) = \sqrt{C} \sum_j v_j \alpha_j \sqrt{f_{\mathrm{SHM}}(v_j)\Delta v} \sin(\omega_j t + \varphi_j). \tag{3.9'}$$

In an experiment, the data-points would be sampled discretely. Assuming that $N = fT$ data points are collected at a specific frequency f over a time period T, they will be separated by a time spacing of $\Delta t = 1/f$, so that the discrete acceleration can be written as:

$$a^n_\phi = \sqrt{C} \sum_j v_j \alpha_j \sqrt{f_{\mathrm{SHM}}(v_j)\Delta v} \sin(\omega_j n \Delta t + \varphi_j), \tag{3.11}$$

for each data-point $n \in 0, 1, ..., N-1$. The discrete Fourier transform of this acceleration is:

$$a^k_\phi = \sum_{n=0}^{N-1} a^n_\phi e^{-i2\pi kn/N}, \tag{3.12}$$

now with $k \in 0, 1, ..., N-1$. The PSD is defined as [18]:

$$S^k_{aa} = \frac{(\Delta t)^2}{T} |a^k_\phi|^2, \tag{3.13}$$

which with the definition of the Fourier transform in eq. (3.12) becomes:

$$S_{aa}^k = C\frac{(\Delta t)^2}{T}\left|\sum_{n=0}^{N-1}\sum_j v_j\alpha_j\sqrt{f_{\rm SHM}(v_j)\Delta v}\sin(\omega_j n\Delta t+\varphi_j)e^{-i2\pi kn/N}\right|^2. \tag{3.14}$$

To calculate this quantity, it it easier to look at the PSD in terms of angular frequency ω (not to be confused with the angular frequency ω_j of the scalar field). Using that $k=\omega T/(2\pi)=\omega\Delta tN/(2\pi)$, the PSD takes the form:

$$S_{aa}(\omega) = C\left|\sum_j v_j\alpha_j\sqrt{\frac{f_{\rm SHM}(v_j)\Delta v}{T}}\Delta t\sum_{n=0}^{N-1}\sin(\omega_j n\Delta t+\varphi_j)e^{-i\omega n\Delta t}\right|^2. \tag{3.15}$$

By noting that the experimental frequency resolution Δf depends on the time period T as $\Delta f = 1/T$, this expression can be simplified somewhat. With the definition of ω_j, and large enough T, the frequency resolution can then be approximated as $\Delta f = 1/T \approx m_\phi v_j\Delta v/(2\pi)$, leading to:

$$S_{aa}(\omega) = C\left|\sum_j v_j\alpha_j\Delta v\sqrt{\frac{f_{\rm SHM}(v_j)m_\phi v_j}{2\pi}}\Delta t\sum_{n=0}^{N-1}\sin(\omega_j n\Delta t+\varphi_j)e^{-i\omega n\Delta t}\right|^2. \tag{3.16}$$

In reality, the time period T will be much larger than most other time-scales connected to the experiment, allowing one to use $T\to\infty$, and as a result also $\Delta v\to dv$ and $\Delta t\to dt$. The sum over j then becomes an integral over v:

$$S_{aa}(\omega) = C\left|\int dv v\alpha_v\sqrt{\frac{f_{\rm SHM}(v)m_\phi v}{2\pi}}dt\sum_{n=0}^{N-1}\sin(\omega_v ndt+\varphi_v)e^{-i\omega ndt}\right|^2, \tag{3.17}$$

where the index j is now replaced with v for α and φ, as these will have been randomly drawn for each value of v in the integral. The sum over n can be rewritten and expanded to first order using $(\omega_v\pm\omega)dt << 1$:

$$\begin{aligned} dt\sum_{n=0}^{N-1}\sin(\omega_v ndt+\varphi_v)e^{-i\omega ndt} &= \frac{dt}{2i}\Bigg(e^{i\varphi_v}\cdot\frac{e^{i(\omega_v-\omega)T}-1}{e^{i(\omega_v-\omega)dt}-1}- \\ &- e^{-i\varphi_v}\cdot\frac{1-e^{-i(\omega_v+\omega)T}}{1-e^{-i(\omega_v+\omega)dt}}\Bigg) \approx \frac{i}{2}e^{i(\varphi_v+(\omega_v-\omega)T/2)}\Bigg(-\frac{\sin((\omega_v-\omega)T/2)}{\frac{1}{2}(\omega_v-\omega)}+ \\ &+ e^{-i(2\varphi_v+\omega_v T)}\cdot\frac{\sin((\omega_v+\omega)T/2)}{\frac{1}{2}(\omega_v+\omega)}\Bigg). \end{aligned} \tag{3.18}$$

Taking the limit $(\omega_v\pm\omega)T\to\infty$ and using $\lim_{\varepsilon\to0}\sin(x/\varepsilon)/x=\pi\delta(x)$ leads to

$$\begin{aligned} dt\sum_{n=0}^{N-1}\sin(\omega_v ndt+\varphi_v)e^{-i\omega ndt} &\approx \frac{i\pi}{2}e^{i(\varphi_v+(\omega_v-\omega)T/2)}\times \\ &\times\Bigg[-\delta(\frac{1}{2}(\omega_v-\omega))+\delta(\frac{1}{2}(\omega_v+\omega))\Bigg]. \end{aligned} \tag{3.19}$$

Keeping only the the term associated with positive frequencies (since $\omega, \omega_v > 0$) yields a short expression for the sum:

$$dt \sum_{n=0}^{N-1} \sin(\omega_v n dt + \varphi_v) e^{-i\omega n dt} \approx -i\pi e^{i(\varphi_v + (\omega_v - \omega)T/2)} \delta(\omega_v - \omega), \tag{3.20}$$

and eq. (3.17) becomes:

$$S_{aa}(\omega) \approx C \left| - \int dv v \alpha_v \sqrt{\frac{f_{\mathrm{SHM}}(v) m_\phi v}{2\pi}} i\pi e^{i(\varphi_v + (\omega_v - \omega)T/2)} \delta(\omega_v - \omega) \right|^2 . \tag{3.21}$$

To perform this integral, one can first use the relation between the dark matter velocity and angular frequency in eq. (2.2) to rewrite the expression as an integral over ω_v, then use integration rules for delta functions to evaluate the integral. The result is a short and concise expression for the PSD:

$$S_{aa}(\omega) = C \frac{\pi f_{\mathrm{SHM}}(v) v}{2 m_\phi} \alpha^2 \Big|_{v=\sqrt{2\omega/m_\phi - 2}}, \tag{3.22}$$

with C according to eq. (3.10). The v-index on the Rayleigh-distributed number α has been dropped as it is now only a single random number. Since α is exponentially distributed according to eq. (3.7), the PSD in eq. (3.22) is also exponentially distributed [18]:

$$P[S_{aa}(\omega)] = \frac{1}{\lambda_S(\omega)} e^{-S_{aa}(\omega)/\lambda_S(\omega)}, \tag{3.23}$$

with mean

$$\lambda_{\mathrm{S}}(\omega) \equiv \langle S_{aa}(\omega) \rangle = C \frac{\pi f_{\mathrm{SHM}}(v) v}{m_\phi} \Big|_{v=\sqrt{2\omega/m_\phi - 2}}. \tag{3.24}$$

In any experiment, one can expect some sort of background noise to manifest in the data set. In general, the noise could come from a variety of sources, the two most prominent ones being thermal noise and measurement-added noise [15]. If the background is assumed to be Gaussian in nature (as in the case of thermal noise), it would have an exponentially distributed PSD with mean λ_{B}. With both the individual dark matter signal PSD of eq. (3.22) and background PSD being exponentially distributed, one can show that the total PSD, $S_{aa}^{k,\mathrm{tot}}$, of signal plus background is also exponentially distributed (which is done in appendix A of [18]) and that the total mean is:

$$\lambda(\omega) = \lambda_{\mathrm{S}}(\omega) + \lambda_{\mathrm{B}} = C \frac{\pi f_{\mathrm{SHM}}(v) v}{m_\phi} \Big|_{v=\sqrt{2\omega/m_\phi - 2}} + \lambda_{\mathrm{B}}. \tag{3.25}$$

Knowing that the full data set d of signal, arising from eq. (3.9), plus background noise is exponentially distributed makes it possible to construct a likelihood function that constrains a model $\mathcal{M}$ with model parameters $\boldsymbol{\theta}$ for the signal and background. The data set here is assumed to be given by N measured acceleration points of the test object for each mass of the scalar boson at time intervals Δt. The PSD

distribution of this data set would be measured at frequencies given by $\omega = 2\pi k/T$ for $k \in 0, 1, ..., N-1$, yielding a likelihood function for the model $\mathcal{M}$:

$$\mathcal{L}(d|\mathcal{M}, \boldsymbol{\theta}) = \prod_{k=1}^{N-1} \frac{1}{\lambda_k(\boldsymbol{\theta})} e^{-S_{aa}^{k,\mathrm{tot}}/\lambda_k(\boldsymbol{\theta})}. \tag{3.26}$$

The index k denotes quantities evaluated at a frequency $\omega = 2\pi k/T$, and $\boldsymbol{\theta}$ include parameters describing the signal, such as the coupling constant $y_{\phi n}$ and the velocity distribution $f_{\mathrm{SHM}}(v)$, as well as parameters determining the background contribution. Note that the $k = 0$ mode has been omitted in eq. (3.26). This is because the signal could not contribute to this mode, as the velocity distribution in eq. (3.8) is imaginary for $k = 0$. This mode would therefore only give a constant contribution to the background, which can always be neglected without loss of experimental sensitivity [18].

Having concluded a full likelihood framework, the likelihood function in (3.26) can then be used to statistically infer the achievable experimental sensitivity by setting a discovery and exclusion limit of the scalar-neutron coupling constant. This is the subject of the next chapter.

4

Experimental sensitivity

In the potential experiment searching for dark matter suggested in Section 1.2, one would like to know the limits for which one can either say that detection of a dark matter signal is possible or not. These limits determine the needed sensitivity of the experiment and are termed exclusion limit, for likely exclusion of a signal, and discovery limit for which one can claim the discovery of a signal. Determining these limits is the focus of this chapter, in which a similar approach to [18] was made. To help do this, a frequentist based analysis was performed, using two test statistics. The analysis tested two models, one in which there is no signal (only background), and one in which there is a signal and background. The purpose of the test statistics was then be able to determine which of these models would fit the data best.

4.1 Introducing limits and test statistics

The limits for dismissing or confirming the possibility of a signal are more specifically limits set on the value the coupling constant $y_{\phi n}$. The reason for wanting limits on $y_{\phi n}$ is that this constant determines the interaction strength of the dark matter with the neutrons in the test object, and therefore with the object itself. The discovery limit is therefore the lowest value of this coupling constant needed for which one can say with some certainty that the interaction can be detected in an experiment. Measuring a believed signal with this value as minimum for $y_{\phi n}$ in an experiment would then mean that an actual signal for this type of hypothesised dark matter has been detected.

When setting an exclusion limit, however, the goal is to see at which values of the coupling constant the background can be said to overshadow a signal so that a signal could not be detected. The limit set on $y_{\phi n}$ is then an upper limit on its value, as one seeks to determine the highest value of the coupling constant for which one can still say with some certainty that there is no signal and only background. Above this limit, one can lean in favour of the dark matter hypothesis if a believed signal is detected, but not claim discovery until one reaches the discovery limit.

4.1.1 The profile likelihood

The basic object for calculating the limiting values of the coupling constant is the likelihood function in eq. (3.26) developed in Chapter 3. From this likelihood stems

the frequentist tools in the form of two test statistics that will be used to set the limits. The form of the likelihood that will be used is the profile likelihood:

$$\Theta(m_\phi, C) = 2[\log \mathcal{L}(d|\mathcal{M}, \{C, m_\phi, \hat{\boldsymbol{\theta}}_{\mathrm{B}}\}) - \log \mathcal{L}(d|\mathcal{M}_{\mathrm{B}}, \hat{\boldsymbol{\theta}}_{\mathrm{B}})]. \tag{4.1}$$

Here, some explanation is required. First of all, calculating limits for the coupling constant is effectively the same as first limiting the constant C defined in eq. (3.10), and makes for easier notation. When limits have been found for C, eq. (3.10) can be used to get the limits for $y_{\phi n}$. Secondly, the mass m_ϕ of the dark matter will affect the results of the limits. Hence, both C and m_ϕ are important parameters to consider and are therefore explicitly stated in the expression of the profile likelihood.

In eq. (4.1), $\mathcal{M}$ denotes the model that has been constructed under previous chapters, in which bosonic scalar dark matter hypothetically exists and can be detected as a signal. $\mathcal{M}_{\mathrm{B}}$ instead denotes a model in which no such dark matter exists and there is only background sources. In this model, the coupling constant is zero and hence $C = 0$. The variable $\hat{\boldsymbol{\theta}}_{\mathrm{B}}$ denotes the background parameters with values that maximise the likelihood for that specific data-set d and model.

The profile likelihood in eq. (4.1) is central in the coming definitions of the test statistics, as it encodes the properties of the dark matter. Explicitly, using the derived likelihood in eq. (3.26), it has the form:

$$\Theta(m_\phi, C) = 2 \sum_{k=1}^{N-1} \left[S_{aa}^{k,\mathrm{tot}} \left(\frac{1}{\lambda_{\mathrm{B}}} - \frac{1}{\lambda_k} \right) - \log \frac{\lambda_k}{\lambda_{\mathrm{B}}} \right], \tag{4.2}$$

with λ_k being the mean of the PSD for signal and background as in equation (3.25), and λ_{B} the mean for background only. The data is represented by the total PSD S_{aa}^k, and the statistical behaviour of the data is encoded in the random number α, which is Rayleigh-distributed according to eq. (3.7).

4.1.2 Definitions of the test statistics

For establishing an upper exclusion limit on C (or $y_{\phi n}$), the following test statistic is defined [18, 31]:

$$q_{\mathrm{e}}(m_\phi, C) = \begin{cases} \Theta(m_\phi, C) - \Theta(m_\phi, \hat{C}) & C \geq \hat{C}, \\ 0 & C < \hat{C}. \end{cases} \tag{4.3}$$

$\hat{C}$ is the value of C that maximises the profile likelihood $\Theta(m_\phi, C)$ at a fixed mass m_ϕ. The reason for setting the test statistic to zero for $C < \hat{C}$ is that only values of C larger than the best fit $\hat{C}$ would indicate that the background-only model $\mathcal{M}_{\mathrm{B}}$ is incompatible with the data because the signal model $\mathcal{M}$ is a better fit [31]. While $C < \hat{C}$ would still be considered evidence against the background-only model $\mathcal{M}_{\mathrm{B}}$, it would not be considered evidence in favour of the signal model $\mathcal{M}$, and as such the test statistic can be set to zero for this case. The definition then shows that this test statistic stands for the degradation of the likelihood as C is increased beyond

the best fit point $\hat{C}$ for the model $\mathcal{M}_{\mathrm{B}}$. Note also that q_{e} is defined to be negative.

For the discovery limit, a second test statistic is defined as [18, 31]:

$$q_{\mathrm{d}}(m_\phi) = \Theta(m_\phi, \hat{C}), \tag{4.4}$$

which is a quantity that describes how much the model $\mathcal{M}$, which includes the scalar dark matter boson, fits better to the data than the model $\mathcal{M}_{\mathrm{B}}$ without the scalar. In general, one can say that a larger value of q_{d} means that the model $\mathcal{M}$ with the scalar is more preferred.

4.2 The Asimov method

In an actual experiment, the profile likelihood in eq. (4.1) can be used directly to determine the probability of a signal in an experimental data set. The purpose of the test statistics defined above, however, is to make it possible to find out what the expected sensitivity of the experiment is before it is carried out, through exclusion and discovery limits. This is often done through Monte Carlo simulations of the experiment, from which the expected distributions of q_{e} and q_{d} can be deduced over many simulated data sets. The distributions can, however, also be deduced analytically, as done in [18], which in turns follows likelihood-based statistical tests developed in [31]. This thesis follows this approach, in which the expected sensitivity was calculated analytically with the use of a method utilising the so called Asimov data set [31]. This set is an artificial replacement representative for all the simulated data sets obtained through simulations, and is defined such that when used to evaluate the parameter estimators the true parameter values are obtained [31]. Using the Asimov data set, one can therefore analytically derive asymptotic distributions of the test statistics, otherwise deduced from many runs of a simulation, from which expected exclusion and discovery limits can be calculated.

Since the profile likelihood is central in both definitions of the test statistics, a natural step towards finding exclusion and discovery limits through the Asimov method is to first find the profile likelihood's asymptotic distribution. With the Asimov method on this particular problem, the data set $S_{aa}^{k,\mathrm{tot}}$ is assumed to contain a signal and set to equal the mean prediction of the dark matter model, neglecting statistical fluctuations [18]:

$$S_{aa}^{k,\mathrm{Asimov}} \equiv \lambda_k^{\mathrm{t}} = C_{\mathrm{t}} \frac{\pi f_{\mathrm{SHM}}(v) v}{m_\phi} + \lambda_{\mathrm{B}}. \tag{4.5}$$

The index t indicates that the parameter takes the true value, as per definition of the Asimov data set. This is the same relation as eq. (3.25), and this expression should also be evaluated at $v = \sqrt{4\pi k/(m_\phi T) - 2}$. With this artificial data set, the profile likelihood takes the asymptotic form $\tilde{\Theta}(m_\phi, C)$:

$$\tilde{\Theta}(m_\phi, C) = 2 \sum_{k=1}^{N-1} \left[\lambda_k^{\mathrm{t}} \left(\frac{1}{\lambda_{\mathrm{B}}} - \frac{1}{\lambda_k} \right) - \log \frac{\lambda_k}{\lambda_{\mathrm{B}}} \right], \tag{4.6}$$

with maximum at $C = C_{\mathrm{t}}$:

$$\max_{C} \tilde{\Theta}(m_\phi, C) = \tilde{\Theta}(m_\phi, C_{\mathrm{t}}). \tag{4.7}$$

Assuming that the experiment has run long enough for the width of the frequency bins to be much smaller than the range over which λ_k or λ_{B} varies, the sum over k modes can be approximated into an integral over v. Using eqs. (3.25) and (4.5), and the relation between v and k:

$$\begin{aligned}
\tilde{\Theta}(m_\phi, C) = \frac{m_\phi T}{\pi} \int dv v \Bigg[\left(C_{\mathrm{t}} \frac{\pi f_{\mathrm{SHM}}(v) v}{m_\phi} + \lambda_{\mathrm{B}} \right) \left(\frac{1}{\lambda_{\mathrm{B}}} - \frac{1}{C_{\mathrm{t}} \frac{\pi f_{\mathrm{SHM}}(v) v}{m_\phi} + \lambda_{\mathrm{B}}} \right) - \\
- \log \left(1 + C \frac{\pi f_{\mathrm{SHM}}(v) v}{m_\phi \lambda_{\mathrm{B}}} \right) \Bigg] = \\
= \frac{m_\phi T}{\pi} \int dv v \Bigg[C_{\mathrm{t}} \frac{\pi f_{\mathrm{SHM}}(v) v}{m_\phi \lambda_{\mathrm{B}}} + \frac{C_{\mathrm{t}} \frac{\pi f_{\mathrm{SHM}}(v) v}{m_\phi \lambda_{\mathrm{B}}}}{C \frac{\pi f_{\mathrm{SHM}}(v) v}{m_\phi \lambda_{\mathrm{B}}} + 1} + 1 - \frac{1}{C_{\mathrm{t}} \frac{\pi f_{\mathrm{SHM}}(v) v}{m_\phi \lambda_{\mathrm{B}}} + 1} - \\
- \log \left(1 + C \frac{\pi f_{\mathrm{SHM}}(v) v}{m_\phi \lambda_{\mathrm{B}}} \right) \Bigg].
\end{aligned} \tag{4.8}$$

In any individual frequency bin, an eventual signal will most likely be much smaller than the background, $C\pi f_{\mathrm{SHM}}(v)v/m_\phi$, $C_{\mathrm{t}}\pi f_{\mathrm{SHM}}(v)v/m_\phi << \lambda_{\mathrm{B}}$, allowing one to expand eq. (4.8) to leading order in C and C_{t}. This yields the simplified expression

$$\tilde{\Theta}(m_\phi, C) \approx \frac{CT\pi}{m_\phi} \left(C_{\mathrm{t}} - \frac{C}{2} \right) \int dv v^3 \frac{f^2_{\mathrm{SHM}}(v)}{\lambda^2_{\mathrm{B}}}. \tag{4.9}$$

If the background is frequency independent, λ_{B} can be extracted from the integral:

$$\tilde{\Theta}(m_\phi, C) \approx \frac{CT\pi}{m_\phi \lambda^2_{\mathrm{B}}} \left(C_{\mathrm{t}} - \frac{C}{2} \right) \int dv v^3 f^2_{\mathrm{SHM}}(v). \tag{4.10}$$

As the background to be used in Chapter 5 is the thermal acceleration noise of the proposed experiment of Section 1.2, a frequency independent background can be assumed from now on, since the acceleration noise is seen to be frequency independent in eq. (1.1). Eq. (4.10) is the final asymptotic form of the profile likelihood and is used in coming sections to derive exclusion and discovery limits.

4.3 Exclusion limit

The goal of this section is to derive an upper exclusion limit for the coupling constant $y_{\phi n}$ for which a signal can be rejected; in other words rejecting the dark matter plus background model $\mathcal{M}$ in favour of the background-only model $\mathcal{M}_{\mathrm{B}}$. In this case, the Asimov data set to use is a background-only distribution, in which $C_{\mathrm{t}} = 0$. In accordance with most high-energy physics experiments, the confidence interval chosen for excluding a signal is 95%, corresponding to a p-value no larger than 0.05 [32]. Only a one-sided p-value is considered, as any downward fluctuations of the background mean would not be considered evidence *against* the background.

4.3.1 The value of q_{e}

From the definition of the test statistic in eq. (4.3), and using the maximum of eq. (4.7), the test statistic for the 95% exclusion limit of a signal takes the simple form

$$q_{\mathrm{e}}(m_\phi, C_{95\%}) = \begin{cases} \tilde{\Theta}(m_\phi, C_{95\%}) & C > \hat{C}, \\ 0 & C \leq \hat{C}. \end{cases} \tag{4.11}$$

Having this equality with the asymptotic profile likelihood, one would like to use the asymptotic distribution of the test statistic to find the value of q_{e} at a 95% confidence interval, and from there use eq. (4.11) to calculate the explicit upper limit $C_{95\%}$.

The asymptotic distribution of the test statistic q_{e} is in this case straightforward to deduce using Wilks' theorem [33]. The probability density function (PDF) of this test statistic is according to Wilks' theorem asymptotically a half-chi-squared distribution with one degree of freedom, at a fixed mass m_ϕ (only half from the definition of q_{e}) [31]. An explicit form of the PDF is given in [31] but for a test statistic defined with opposite sign, from which the PDF for q_{e} in this thesis can be seen to be:

$$f(q_{\mathrm{e}}) = \frac{1}{2}\delta(-q_{\mathrm{e}}) + \frac{1}{2}\frac{1}{\sqrt{2\pi}}\frac{1}{\sqrt{-q_{\mathrm{e}}}}e^{q_{\mathrm{e}}/2}. \tag{4.12}$$

Its cumulative distribution function (CDF) is then found to be equal to that of the standard normal distribution with respect to the square root of minus q_{e}:

$$F(q_{\mathrm{e}}) = \Phi(\sqrt{-q_{\mathrm{e}}}). \tag{4.13}$$

The p-value is then given by [31]:

$$p = 1 - F(q_{\mathrm{e}}) = 1 - \Phi(\sqrt{-q_{\mathrm{e}}}). \tag{4.14}$$

Having chosen to find the exclusion limit with a confidence interval of 95%, the p-value can be set to 0.05 to find the corresponding value of q_{e}:

$$q_{\mathrm{e}}^{95\%} = q_{\mathrm{e}}(m_\phi, C_{95\%}) = -(\Phi^{-1}[0.95])^2 \approx -2.71. \tag{4.15}$$

4.3.2 The upper limit of $y_{\phi n}$

Now having explicit forms for both sides of eq. (4.11), the upper exclusion limit on $y_{\phi n}$ can be explicitly calculated. Using the asymptotic form of the profile likelihood in (4.10), with $C_{\mathrm{t}} = 0$, and $q_{\mathrm{e}}^{95\%}$ in eq. (4.15) with no statistical variations, the upper limit on C becomes:

$$C_{95\%} = \sqrt{\frac{-2 \cdot q_{\mathrm{e}}^{95\%} \cdot m_\phi \lambda_{\mathrm{B}}^2}{T\pi}\left[\int dv v^3 f_{\mathrm{SHM}}^2(v)\right]^{-1}}. \tag{4.16}$$

Solving for the coupling constant in (3.10), the form of the 95% exclusion limit of $y_{\phi n}$ becomes:

$$y_{\phi n}^{95\%} = x_{\mathrm{t.o}} m_{\mathrm{n}} \sqrt{\frac{\lambda_{\mathrm{B}}}{\rho_{\mathrm{DM}}}} \left(\frac{-2 \cdot q_{\mathrm{e}}^{95\%} \cdot m_\phi}{T\pi} \left[\int dv v^3 f_{\mathrm{SHM}}^2(v) \right]^{-1} \right)^{1/4}. \tag{4.17}$$

Note that the integral over velocity should be evaluated from 0 to ∞, giving an analytic result of

$$\begin{aligned} &\int_0^\infty dv v^3 f_{\mathrm{SHM}}^2(v) = \frac{e^{-2v_{\mathrm{obs}}^2/v_0}}{8\pi}(9v_0^2 + 4v_{\mathrm{obs}}^2) + \\ &+ \frac{\sqrt{2\pi}}{32\pi v_0 v_{\mathrm{obs}}}(15v_0^4 + 40v_0^2 v_{\mathrm{obs}}^2 + 16v_{\mathrm{obs}}^4) \operatorname{erf}\left[\frac{\sqrt{2} v_{\mathrm{obs}}}{v_0} \right] \approx 1.003 \cdot 10^{-6}, \end{aligned} \tag{4.18}$$

that can be used to get a concrete expression for $y_{\phi n}^{95\%}$. In the next chapter, this result is used to show how $y_{\phi n}^{95\%}$ varies with different values on the mass m_ϕ, using realistic values of λ_{B} and $x_{\mathrm{t.o}}$ based on the QTL experiment.

4.4 Discovery limit

Having a 95% exclusion limit for which a signal can be rejected in favour of only background, the next step is to find the lower limit of $y_{\phi n}$ for which the background is rejected in favour of the signal plus background model. Rejecting the background model at a level of 5σ would be considered a discovery, corresponding to a p-value of $2.87 \cdot 10^{-7}$ [32]. As for the exclusion limit, only a one-sided p-value is considered since any upward fluctuations of the hypothesised signal mean would not be considered evidence *against* the signal.

Finding an expression for the discovery limit $y_{\phi n}^{5\sigma}$ is straightforward. With the definition of q_{d} in eq. (4.4) and the same asymptotic form of the profile likelihood in eq. (4.10), with $C_{\mathrm{t}} = \hat{C}$, one obtains the same expression as for the exclusion limit but with a sign difference and another value of the test statistic:

$$y_{\phi n}^{5\sigma} = x_{\mathrm{t.o}} m_{\mathrm{n}} \sqrt{\frac{\lambda_{\mathrm{B}}}{\rho_{\mathrm{DM}}}} \left(\frac{2 \cdot q_{\mathrm{d}}^{5\sigma} \cdot m_\phi}{T\pi} \left[\int dv v^3 f_{\mathrm{SHM}}^2(v) \right]^{-1} \right)^{1/4}. \tag{4.19}$$

The threshold value $q_{\mathrm{d}}^{5\sigma}$ giving the discovery limit is not as easily calculated as $q_{\mathrm{e}}^{95\%}$, and will be seen to be more experiment dependent.

4.4.1 The value of q_{d}

To obtain the value $q_{\mathrm{d}}^{5\sigma}$, one must first know the asymptotic distribution of the test statistic, specifically the distribution under the assumption of background only. This distribution determines how likely the background is to produce a value for q_{d}, which gives a lower threshold limit $q_{\mathrm{d}}^{5\sigma}$ that should be set to claim discovery of a signal. However, unlike with the test statistic for exclusion, Wilks' theorem cannot directly be used to determine the asymptotic distribution, as q_{d} has zero degrees of freedom (instead of one). In order for Wilks' theorem to be applicable to this

definition of the test statistic, certain assumptions must be made that allows one to find an alternative form of q_d via a change of variables. This is done explicitly in Appendix D in [18], where they show that the asymptotic distribution of q_d is actually also half-chi-squared with one degree of freedom:

$$f(q_\mathrm{d}) = \frac{1}{2}\delta(q_\mathrm{d}) + \frac{1}{2}\frac{1}{\sqrt{2\pi}}\frac{1}{\sqrt{q_\mathrm{d}}}e^{-q_\mathrm{d}/2}. \tag{4.20}$$

Note the sign difference to eq. (4.12) with q_e defined to be negative. The associated CDF is similarly

$$F(q_\mathrm{d}) = \Phi(\sqrt{q_\mathrm{d}}), \tag{4.21}$$

but with opposite sign inside the square-root. The Asimov data set to use is background-only distributed, since the threshold value $q_\mathrm{d}^{5\sigma}$ searched for comes from the asymptotic background-only distribution of q_d. In practice, this means that the data set is assumed to contain only background, but that there could be an upward fluctuation in some frequency range that is better described by the model including the dark matter signal. Realistically, in an experiment a number of independent frequency windows would be scanned, corresponding to different scalar boson masses, and in any of these windows, an upward fluctuation could occur [18]. One would therefore like to know the probability of the background "faking" a signal with such a fluctuation in any of these bins. The possibility of this happening is called the look-elsewhere effect, and arises because the scanned frequency space is so large that the chance of a statistically insignificant fluctuation in not negligible. Dividing the frequency space into smaller windows minimises this effect. The probability of a "faked" signal is given by the survival function [18]:

$$S[q_\mathrm{d}^{5\sigma}] = 1 - F(q_\mathrm{d}^{5\sigma}) = 1 - \Phi(\sqrt{q_\mathrm{d}^{5\sigma}}), \tag{4.22}$$

describing the chance that the test statistic takes a value greater than $q_\mathrm{d}^{5\sigma}$, under the assumption of background-only. Under the assumption of N_m individually scanned frequency bins, $q_\mathrm{d}^{5\sigma}$ needs to be set so that the probability of the background faking the signal in any bin is $1 - p_{5\sigma}$, with $p_{5\sigma} \sim 2.87 \cdot 10^{-7}$ for a 5σ significance level. Since $p_{5\sigma}$ is very small, the probability that at least one value of q_d is greater than $q_\mathrm{d}^{5\sigma}$ in any frequency set is

$$p_{5\sigma} = 1 - (1 - S[q_\mathrm{d}^{5\sigma}])^{N_m} \approx N_m S[q_\mathrm{d}^{5\sigma}], \tag{4.23}$$

where the approximation uses a Taylor approximation around $S[q_\mathrm{d}^{5\sigma}] << 1$. This with eq. (4.22) leads to

$$q_\mathrm{d}^{5\sigma} = \left[\Phi^{-1}\left(1 - \frac{p_{5\sigma}}{N_m}\right)\right]^2. \tag{4.24}$$

Determining $q_\mathrm{d}^{5\sigma}$ then requires knowing the number of scanned bins N_m. Estimating a proper value for N_m is hard, however, since a continuum of frequencies can be scanned in practice, even if not all points have independent data. A mass point described by the frequency $\omega_\phi \approx m_\phi$ is expected to have a bandwidth related to its escape velocity:

$$\delta\omega_\phi = \frac{1}{2} m_\phi v_{esc}^2 \sim m_\phi v_0^2, \tag{4.25}$$

with $v_{esc} \sim v_0$ (the speed of the local rotation curve) in the SHM [18]. A set of independent mass points can then be characterised by the relation [18]:

$$m_\phi^{(i)} = m_\phi^{(0)}(1 + \beta v_0^2)^i, \tag{4.26}$$

with $i = 0, ..., N_m - 1$. The parameter β is a number of order unity that can be tuned to Monte Carlo simulations. Tuning β for larger p-values in simulations allows one to analytically extrapolate to smaller p-values, for which the number of simulations would not be manageable to calculate $q_{\mathrm{d}}^{5\sigma}$ directly. This step is not done in this thesis, but β has been simulated to $\beta \approx 3/4$ in [18] with bandwidth $\beta v_0 v_{\mathrm{obs}}$. Here, a similar value is used, revised to fit with the used bandwidth of βv_0^2, so that $\beta \approx 3/4 \cdot v_{\mathrm{obs}}/v_0 \approx 0.791$. N_m can then be estimated by relating $m_\phi^{(0)}$ with the minimum frequency $\omega_{\phi,\mathrm{min}}$ and $m_\phi^{(N_m-1)}$ with the highest frequency $\omega_{\phi,\mathrm{max}}$ and taking the logarithm on both sides of eq. (4.26):

$$\begin{aligned}
&\log \frac{\omega_{\phi,\mathrm{max}}}{\omega_{\phi,\mathrm{min}}} = \log \frac{m_\phi^{(N_m-1)}}{m_\phi^{(0)}} = \log\Big(1 + \beta v_0^2\Big)^{(N_m-1)} = \\
&= (N_m - 1) \log\Big(1 + \beta v_0^2\Big) \approx N_m \log\Big(1 + \beta v_0^2\Big) \approx \\
&\approx N_m \beta v_0^2 \\
&\Rightarrow N_m \approx \frac{1}{\beta v_0^2} \log \frac{\omega_{\phi,\mathrm{max}}}{\omega_{\phi,\mathrm{min}}}.
\end{aligned} \tag{4.27}$$

Using this expression for N_m (for $N_m >> 1$) depending on the chosen frequency span scanned, $q_{\mathrm{d}}^{5\sigma}$ can be estimated with eq. (4.24), which in turn can be used to determine the limit $y_{\phi n}^{5\sigma}$ for the coupling constant in eq. (4.19).

Now having explicit expressions for both the exclusion limit of $y_{\phi n}$ in (4.17) and discovery threshold in (4.19), a full experimental sensitivity estimation can be made, using only the analytical tools and frameworks derived in these past three chapters. The method used here can in principle be applied to any experiment, and any wave dark matter candidate, allowing for a powerful analytical testing of dark matter models without having to run long simulations. The possible application of this on an experiment at QTL is examined in the next chapter, where exclusion and discovery limits for an eventual experiment are shown as a function of mass.

5

Estimations of Exclusion and Discovery Limits

Having concluded a full theoretical framework for the scalar boson candidate, as well as having a statistical framework for testing its interaction strength with a test object, this could then be applied to the proposed experiment at QTL, for which the experimental sensitivity could be estimated. With the relevant equations for exclusion and discovery limits of Chapter 4, these were plotted in Python in a chosen mass interval for the dark matter, using the thermal acceleration noise of eq. (1.1) in Chapter 1 as background term, having chosen to scale the total time period in two ways. The resulting limits of the coupling constant were also compared with result in [24]. The result used for comparison in [24] was an upper limit calculated based on two experiments testing violations of the weak equivalence principle (WEP) for scalar-quark couplings. This is the same type of EP-violation investigated in this thesis for the scalar-neutron interaction. The experiments both measured the differential acceleration of two test objects of different compositions, one in a rotating torsion balance [34] and the other in free fall [35, 36]. The plotted WEP-result was used to compare with results here, modified for a scalar-neutron coupling using the neutron form factor in [26].

5.1 Parameters and variables

In eqs. (4.15) and (4.24), $q_{\mathrm{e}}^{95\%}$ and $q_{\mathrm{d}}^{5\sigma}$ can be seen to depend directly on the mean background term λ_{B}. To make the analytical results relevant for the the proposed experiment at QTL described in Section 1.2, λ_{B} was assumed to be a thermal acceleration noise (exponentially distributed), with values given by eq. (1.1). Two values of the quality factor Q_{m} were assumed, as well as two sizes of the test object, resulting in four background terms $\lambda_{\mathrm{B}} = S_{aa}^{\mathrm{therm}}$ shown in tab. 5.1.

Radius of test object (µm)	$m_{\mathrm{t.o}}$ (kg)	Q_{m}	$\lambda_{\mathrm{B}} = S_{aa}^{\mathrm{therm}}$ (eV)
1	$5 \cdot 10^{-14}$	10^{7}	$8.2 \cdot 10^{-49}$
1	$5 \cdot 10^{-14}$	10^{11}	$8.2 \cdot 10^{-53}$
100	$5 \cdot 10^{-8}$	10^{7}	$8.2 \cdot 10^{-55}$
100	$5 \cdot 10^{-8}$	10^{11}	$8.2 \cdot 10^{-59}$

Table 5.1: Four background terms shown in the rightmost column in natural units of eV, for each size and and quality factor stated in the leftmost columns.

The other variable needed to be set according to experiment was $x_{\text{t.o}}$, describing the ratio of protons and neutrons in the test object. The microspheres levitated at QTL are made of lead. Using the proton number 82 for lead, and standard atomic mass 207.2, $x_{\text{t.o}}$ could be calculated to

$$x_{\text{t.o}} \approx 1 + \frac{82}{207.2 - 82} \approx 1.65.$$

For the discovery limit $q_{\text{d}}^{5\sigma}$, a mass range was also needed, in order to calculate N_m. The whole possible mass range for wave dark matter was not investigated, as the amount of data for such a large range would be unwieldy. Instead a smaller mass interval was chosen with $1.24 \cdot 10^{-13}$ eV $\leq m_\phi \leq 4.14 \cdot 10^{-12}$ eV, corresponding to frequencies of 30 Hz up to 1 kHz that could be probed in the experiment at QTL. With eqs. (4.27) and (4.24), $q_{\text{d}}^{5\sigma}$ could then be calculated to be approximately 56.1. The maximum frequency of 1 kHz was optimistically chosen. A lower maximum of 200 Hz, corresponding to a mass $8.27 \cdot 10^{-13}$, would perhaps be more realistic but the higher one was chosen in order to probe a larger mass range, and to compare with result in [24].

The variable T in eqs. (4.15) and (4.24) stands for the time period for each frequency f being scanned, corresponding to a mass m_ϕ. This means that for each mass bin scanned, with bandwidth $\beta m_\phi v_0^2$ according to the parameterisation in (4.26), the scanning time T could be different. The total time period was chosen to scale with the mass in two ways, in accordance with [18]: $T \propto (m_\phi^i)^{-1}$ and $T \propto (m_\phi^i)^{-5}$. The maximum time T_{max} chosen for the lowest mass bin was 1000 s in both cases, so that T could be parameterised in the following two ways:

$$T^{m^{-1}} = T_{\text{max}} \cdot (m_\phi^0)^1 \cdot (m_\phi^i)^{-1}, \tag{5.1}$$

$$T^{m^{-5}} = T_{\text{max}} \cdot (m_\phi^0)^5 \cdot (m_\phi^i)^{-5}, \tag{5.2}$$

with $m_\phi^0 = 1.24 \cdot 10^{-13}$ eV. This lead to the highest mass bin for $T^{m^{-1}}$ being scanned for $T_{\text{min}}^{m^{-1}} = 29.95$ s, and for $T^{m^{-5}}$ the lowest mass bin was scanned for $T_{\text{min}}^{m^{-5}} = 24$ µs.

Using the analytic expression in eq. (4.18), ρ_{DM} =0.4 GeV/cm^3, $m_{\text{n}} = 939.6$ MeV, and parameter values and scalings stated in this section, the exclusion and discovery limits of eqs. (4.17) and (4.19) could be explicitly specified for the proposed experiment at QTL:

$$T^{m^{-1}}: \quad y_{\phi n}^{95\%} = 8.69 \cdot 10^{11}\ \text{eV}^{-1} \cdot \sqrt{\lambda_{\text{B}}} \cdot \sqrt{m_\phi}, \tag{5.3}$$

$$y_{\phi n}^{5\sigma} = 1.84 \cdot 10^{12}\ \text{eV}^{-1} \cdot \sqrt{\lambda_{\text{B}}} \cdot \sqrt{m_\phi}, \tag{5.4}$$

$$T^{m^{-5}}: \quad y_{\phi n}^{95\%} = 7.01 \cdot 10^{24}\ \text{eV}^{-2} \cdot \sqrt{\lambda_{\text{B}}} \cdot \sqrt{m_\phi^3}, \tag{5.5}$$

$$y_{\phi n}^{5\sigma} = 1.48 \cdot 10^{25}\ \text{eV}^{-2} \cdot \sqrt{\lambda_{\text{B}}} \cdot \sqrt{m_\phi^3}. \tag{5.6}$$

The coupling constant can be seen to be proportional to $m_\phi^{1/2}$ or $m_\phi^{3/2}$, with the exclusion and discovery case differing only by a proportionality constant.

5.2 Results and comparison with WEP

Plots of the resulting exclusion and discovery limits from eqs. (5.3)–(5.6) are shown in figs. 5.1 and 5.2. Fig. 5.1 shows estimated limits for the time period scaling $T^{m^{-1}}$ of eq. (5.1), plotted against the scalar boson mass, for the four different background terms. Fig. 5.2 shows the same for the time period scaling $T^{m^{-5}}$ of eq. (5.2).

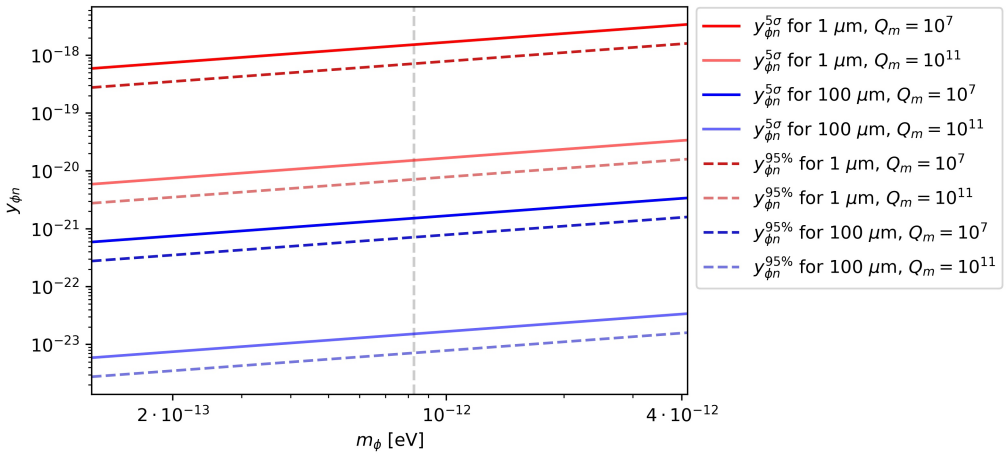

Figure 5.1: Exclusion and discovery limits with $T^{m^{-1}}$ plotted against the mass m_ϕ, for four different backgrounds. Solid lines are discovery limits $q_{\mathrm{d}}^{5\sigma}$ and dashed lines are exclusion limits $q_{\mathrm{e}}^{95\%}$, colour coded with red lines indicating the smaller test object and blue lines the larger test object, each with two different mechanical quality factors. The vertical grey line at 200 Hz indicate the lower maximum frequency perhaps more realistic for the experiment at QTL.

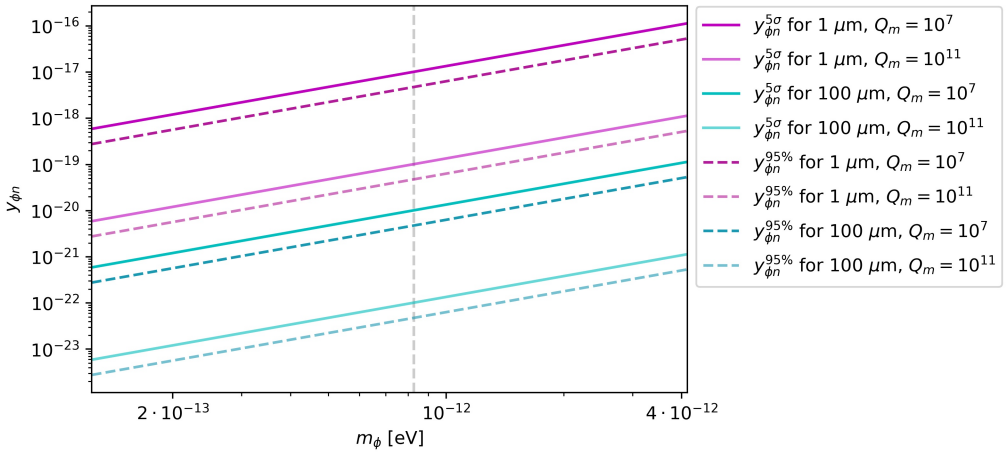

Figure 5.2: Exclusion and discovery limits with $T^{m^{-5}}$ plotted against the mass m_ϕ, for four different backgrounds. Solid lines are discovery limits $q_{\mathrm{d}}^{5\sigma}$ and dashed lines are exclusion limits $q_{\mathrm{e}}^{95\%}$, colour coded with magenta lines indicating the smaller test object and cyan lines the larger test object, each with two different mechanical quality factors. The vertical grey line at 200 Hz indicate the lower maximum frequency perhaps more realistic for the experiment at QTL.

Solid lines represent discovery limits from eqs. (5.4) and (5.6), and dashed lines represent exclusion limits from eqs. (5.3) and (5.5). The top two results in red or magenta in each figure are limits for the smaller test object with radius 1 µm, and results in blue or cyan are limits for the larger test object with radius 100 µm. The dashed vertical grey line indicate where the lower maximum frequency of 200 Hz would cut of the results, here plotted up to 1 kHz.

As can be seen directly from eqs. (5.3)–(5.6), the results scale with the square root of the background, so that lower background gives a higher sensitivity in the form of lower limit values. Also visible from these equations is the fact that the $T^{m^{-5}}$ scaling will result in a faster loss of sensitivity for higher masses compared to the $T^{m^{-1}}$ scaling, which is seen as a steeper slope of the plots in fig. 5.2 compared to that of fig. 5.1. The sensitivity lessens for higher masses in both cases, however, as both scalings results in higher coupling constant values for higher scalar masses.

Comparisons of results with the WEP result are shown in figs. 5.3 and 5.4, but only with discovery and exclusion limits for the smaller test object and $Q_{\mathrm{m}} = 10^7$, giving the highest thermal background contribution. The dashed green line is the WEP upper limit, replotted for a scalar-neutron coupling with the use of a neutron form factor and the web-based tool Plot Digitizer. The plot includes only the minimally obtained limit for each mass from two calculated results for the two experiments. As before, the vertical grey line indicate where the lower maximum frequency of 200 Hz would cut of the results, which would be just after the change in slope of the WEP result.

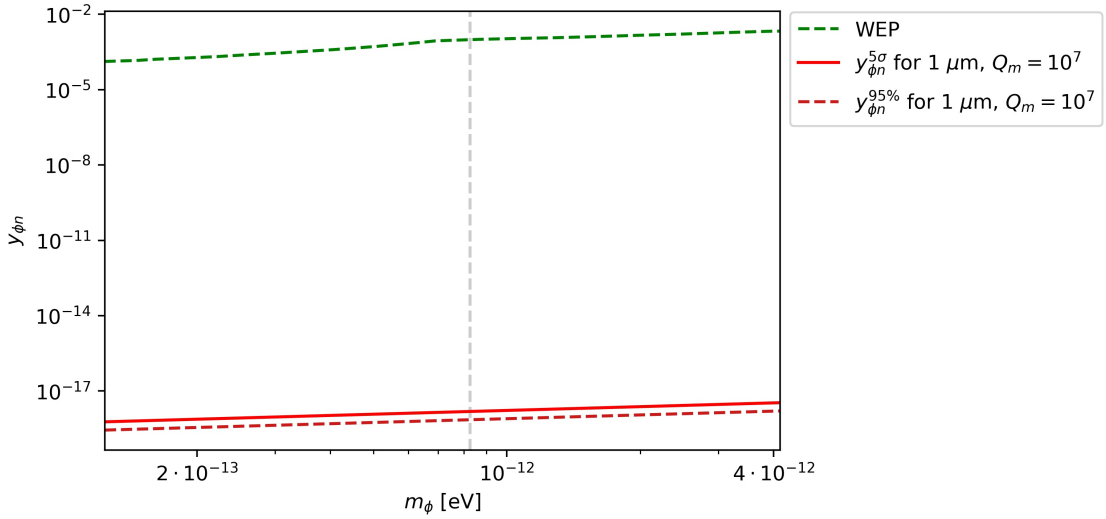

Figure 5.3: Exclusion and discovery limits with $T^{m^{-1}}$ for the smallest test object with mechanical quality factor 10^7, giving the highest background. The WEP exclusion limit is plotted in a dashed green line for comparison. The vertical grey line at 200 Hz indicate the lower maximum frequency perhaps more realistic for the experiment at QTL.

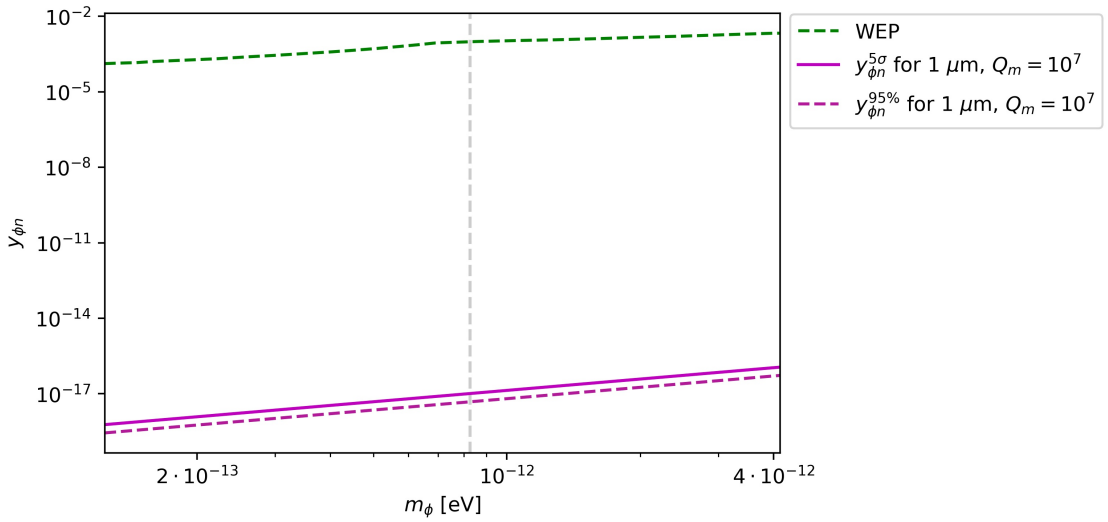

Figure 5.4: Exclusion and discovery limits with $T^{m^{-5}}$ for the smallest test object with mechanical quality factor 10^7, giving the highest background. The WEP exclusion limit is plotted in a dashed green line for comparison. The vertical grey line at 200 Hz indicate the lower maximum frequency perhaps more realistic for the experiment at QTL.

5.3 Discussion and analysis

Comparisons with the WEP-result show that the proposed experiment at QTL could achieve a higher sensitivity in searching for scalar wave dark matter coupling to neutrons. Both discovery and exclusion limits are well below the WEP exclusion limit by several orders of magnitude, including results for higher masses with the $T^{m^{-5}}$ scaling. The experiment is therefore well motivated for EP-violating acceleration searches of scalar dark matter. Some aspects of the analysis and assumptions made during the derivation of the theoretical framework are worth considering though.

The loss of sensitivity for higher masses with the $T^{m^{-5}}$ scaling implies that this choice of time period would not be as good for searches in larger mass intervals. For very small mass intervals, the loss of sensitivity for larger masses is not as apparent compared to the $T^{m^{-1}}$ scaling, but even for the interval 30–200 Hz the difference is still visible. This shows that the choice of time period has a clear effect on the sensitivity. Choosing to scale the period with mass can result in a large difference in sensitivity for lower and higher masses. Longer periods of scanning for each mass bin will give an overall higher sensitivity, but scanning each bin for 1000 s, for example, might not be feasible in practice, since the total scanning time would be too high for the large amount of bins needed. Higher frequencies, corresponding to higher masses, will however not require as long a scanning period as the lower frequencies to achieve the same sensitivity. Finding a time period scaling that effectively takes this into account could therefore be a good way of optimising the sensitivity.

Furthermore, the scaling of sensitivity with the square root of the background means

that additional background contributions, apart from the thermal acceleration noise, can easily be accounted for, leading only to a shift in results. This assumes, however, that any additional background's PSD would be exponentially distributed so that the total data PSD is exponentially distributed, leading to that the total PSD mean is the sum of signal mean and background mean as in eq. (3.25). If the background would happen to be distributed differently than the signal, a new likelihood function would need to be derived that accounts for this, but the sensitivity analysis done here could just as well be applied to any likelihood. Additionally, the final results for the limits are also based on that the background mean is a constant. In the case of a frequency dependent background, the asymptotic profile likelihood of eq. (4.9) would be needed for calculating exclusion and discovery limits, rather than eq. (4.10).

Some assumptions done in the derivations of the likelihood and sensitivity should also be considered. The assumed velocity distribution $f_{\mathrm{SHM}}(v)$ for the dark matter velocity is taken from the standard halo model, but other models with different distributions could change the resulting sensitivity. In calculating the acceleration PSD, the result was also dependent on that the time period T would be much larger than other time scales in the experiment, allowing for the approximation $T \to \infty$ in eq. (3.17). It is therefore important to make sure that this approximation holds when choosing time period. Since values of the local dark matter density ρ_{DM} varies in literature, the chosen value can also marginally affect the result, and the same goes for the parameter $x_{\mathrm{t.o}}$ that is assumed to only depend on the neutron mass and number of neutron in the test object. Finally, it should be remembered that the framework development and analysis done was for only a scalar-neutron coupling. Since the coupling in its basic form is actually a coupling between the scalar boson and quarks, the analysis would be equally valid by assuming only a scalar-proton coupling or a combination of the two.

In conclusion, the derived experimental sensitivity for the proposed experiment at QTL can be said to be high enough as to motivate actually performing the experiment, especially compared to the similar analysis done in [24] for the same dark matter candidate. While some details need to be carefully chosen and analysed, searching for EP-violating accelerations induced by scalar-neutron couplings can be seen to be possible with this set-up, even allowing for exploration of a previously unexplored parameter space of the scalar boson.

References

[1] A. Arbey and F. Mahmoudi, "Dark matter and the early universe: A review," *Prog. Part. Nucl. Phys.*, vol. 119, 2021. [Online]. Available: https://doi.org/10.1016%2Fj.ppnp.2021.103865

[2] G. Bertone and D. Hooper, "History of dark matter," *Rev. Mod. Phys.*, vol. 90, 2018. [Online]. Available: https://doi.org/10.1103%2Frevmodphys.90.045002

[3] G. Bertone et al., "Particle dark matter: evidence, candidates and constraints," *Phys. Rep.*, vol. 405, 2005. [Online]. Available: https://doi.org/10.1016%2Fj.physrep.2004.08.031

[4] M. Persic et al., "The Universal Rotation Curve of Spiral Galaxies: I. the Dark Matter Connection," *Mon. Not. R. Astron. Soc. 281 (1996) 27*, 1996. [Online]. Available: https://doi.org/10.48550/arXiv.astro-ph/9506004

[5] V. C. Rubin et al., "Extended rotation curves of high-luminosity spiral galaxies. IV. Systematic dynamical properties, Sa through Sc," *Astrophys. J. Lett.*, vol. 225, 1978. [Online]. Available: https://inspirehep.net/literature/1592444

[6] D. N. Schramm and G. Steigman, "Relic Neutrinos and the Density of the Universe," *Astrophys. J.*, vol. 243, 1981. [Online]. Available: https://ui.adsabs.harvard.edu/abs/1981ApJ...243....1S/abstract

[7] M. Davis et al., "A survey of galaxy redshifts. II. The large scale space distribution." *Astrophys. J.*, vol. 253, 1982. [Online]. Available: https://ui.adsabs.harvard.edu/abs/1982ApJ...253..423D/abstract

[8] P. A. R. Ade et al. (Planck coll.), "Planck 2015 results. xiii. cosmological parameters," *Astron. Astrophys.*, vol. 594, 2016. [Online]. Available: https://doi.org/10.1051%2F0004-6361%2F201525830

[9] T. Hambye et al., "Dark matter as a heavy thermal hot relic," *Phys. Lett. B*, vol. 807, 2020. [Online]. Available: https://doi.org/10.1016%2Fj.physletb.2020.135553

[10] Y. Du et al., "Revisiting dark matter freeze-in and freeze-out through phase-space distribution," *Journal of Cosmology and Astroparticle Physics*, vol. 2022, 2022. [Online]. Available: https://doi.org/10.1088%2F1475-7516%2F2022%2F04%2F012

[11] A. Ringwald, "Axions and Axion-Like Particles," 2014. [Online]. Available: https://doi.org/10.48550/arXiv.1407.0546

[12] E. G. M. Ferreira, "Ultra-light dark matter," *Astron. Astrophys. Rev.*, vol. 29, 2021. [Online]. Available: https://doi.org/10.1007%2Fs00159-021-00135-6

[13] T. M. Undagoitia and L. Rauch, "Dark matter direct-detection experiments," *J. Phys. G*, vol. 43, 2015. [Online]. Available: https://doi.org/10.1088%2F0954-3899%2F43%2F1%2F013001

[14] P. W. Graham et al., "Dark matter direct detection with accelerometers," *Phys. Rev. D*, vol. 93, 2016. [Online]. Available: https://doi.org/10.1103%2Fphysrevd.93.075029

[15] D. Carney et al., "Ultralight Dark Matter Detection with Mechanical Quantum Sensors," *New J. Phys.*, vol. 23, 2021. [Online]. Available: https://doi.org/10.1088%2F1367-2630%2Fabd9e7

[16] W. Wieczorek, "Wieczorek lab," [Online; accessed 6 November 2023]. Available: https://wieczorek-lab.com/.

[17] M. Gutierrez Latorre et al., "Superconducting Microsphere Magnetically Levitated in an Anharmonic Potential with Integrated Magnetic Readout," *Phys. Rev. Appl.*, vol. 19, 2023. [Online]. Available: https://link.aps.org/doi/10.1103/PhysRevApplied.19.054047

[18] J. W. Foster et al., "Revealing the Dark Matter Halo with Axion Direct Detection," *Phys. Rev. D*, vol. 97, 2018. [Online]. Available: https://doi.org/10.1103%2Fphysrevd.97.123006

[19] P. F. de Salas et al., "On the estimation of the local dark matter density using the rotation curve of the Milky Way," *J. Cosmol. Astropart. Phys.*, vol. 2019, 2019. [Online]. Available: https://doi.org/10.1088%2F1475-7516%2F2019%2F10%2F037

[20] J. Bovy and S. Tremaine, "On the Local Dark Matter Density," *Astrophys. J.*, vol. 756, 2012. [Online]. Available: https://doi.org/10.1088%2F0004-637x%2F756%2F1%2F89

[21] C. F. McKee et al., "Stars, Gas, and Dark Matter in the Solar Neighbourhood," *Astrophys. J.*, vol. 814, 2015. [Online]. Available: https://doi.org/10.1088%2F0004637x%2F814%2F1%2F13

[22] L. Hui, "Wave dark matter," *Annu. Rev. Astron. Astrophys.*, vol. 59, 2021. [Online]. Available: https://doi.org/10.1146%2Fannurev-astro-120920-010024

[23] A. Arvanitaki et al., "Searching for dilaton dark matter with atomic clocks," *Phys. Rev. D*, vol. 91, 2015. [Online]. Available: https://doi.org/10.1103%2Fphysrevd.91.015015

[24] K. Fukusumi et al., "Upper limit on scalar field dark matter from LIGO-Virgo third observation run," 2023. [Online]. Available: https://doi.org/10.48550/arXiv.2303.13088

[25] M. E. Peskin and D. V. Shroeder, *An Introduction to Quantum Field Theory*, 1st ed. Westview Press, 1995.

[26] M. Cirelli et al., "Tools for model-independent bounds in direct dark matter searches," *J. Cosmol. Astropart. Phys.*, vol. 2013, 2013. [Online]. Available: https://doi.org/10.1088%2F1475-7516%2F2013%2F10%2F019

[27] E. Merzbacher, *Quantum Mechanics*, 3rd ed. John Wiley & Sons, Inc, 1998.

[28] F. Mandl and G. Shaw, *Quantum Field Theory*, 2nd ed. John Wiley & Sons, Ltd, 2010.

[29] J. Frerick et al., "Riding the dark matter wave: Novel limits on general dark photons from LISA Pathfinder," 2024. [Online]. Available: http://dx.doi.org/10.1016/j.physletb.2023.138328

[30] P. Beckmann, "Rayleigh Distribution and Its Generalizations," *J. Res. Natl. Inst. Stand. Technol.*, vol. 68D, 1964. [Online]. Available: https://nvlpubs.nist.gov/nistpubs/jres/68D/jresv68Dn9p927_A1b.pdf

[31] Glen Cowan et al., "Asymptotic formulae for likelihood-based tests of new physics," *Eur. Phys. J. C*, vol. 71, 2011. [Online]. Available: https://arxiv.org/abs/1007.1727

[32] E. Gross, "Practical Statistics for High Energy Physics," *CERN Yellow Rep.: Sch. Proc.*, vol. 3, 2018. [Online]. Available: https://e-publishing.cern.ch/index.php/CYRSP/article/view/1124

[33] J. M. Hardin, "Wilks's Theorem, Global Fits, and Neutrino Oscillations," 2022. [Online]. Available: https://doi.org/10.48550/arXiv.2211.06347

[34] J. Bergé et al., "MICROSCOPE Mission: First Constraints on the Violation of the Weak Equivalence Principle by a Light Scalar Dilaton," *Phys. Rev. Lett.*, vol. 120, 2018. [Online]. Available: https://doi.org/10.1103%2Fphysrevlett.120.141101

[35] P. Touboul et al., "MICROSCOPE mission: Final results of the test of the equivalence principle," *Phys. Rev. Lett.*, vol. 129, 2022. [Online]. Available: http://dx.doi.org/10.1103/PhysRevLett.129.121102

[36] S. Schlamminger et al., "Test of the Equivalence Principle Using a Rotating Torsion Balance," *Phys. Rev. Lett.*, vol. 100, 2008. [Online]. Available: https://doi.org/10.1103%2Fphysrevlett.100.041101

DEPARTMENT OF PHYSICS
CHALMERS UNIVERSITY OF TECHNOLOGY
Gothenburg, Sweden
www.chalmers.se

CHALMERS
UNIVERSITY OF TECHNOLOGY